Intramolecular C−H and N−H Transfer by Ruthenium(II) Amidophosphine Complexes

Michael D. Fryzuk,* Michael J. Petrella, and Brian O. Patrick

Department of Chemistry, University of British Columbia, 2036 Main Mall, Vancouver, BC, Canada, V6T 1Z1

Received July 8, 2005

The formation of ruthenium amidophosphine complexes was accomplished by the addition of $[P_2N_2]Li_2$(Diox) (where P_2N_2 is $PhP(CH_2SiMe_2NSiMe_2CH_2)_2PPh$ and Diox is 1,4-dioxane) to $[RuCl_2(cod)]_x$ to generate $[P_2N_2]Ru(cod)$, or to $RuCl_2(PPh_3)_3$ to generate $[P_2NNH]Ru(C_6H_4PPh_2)$. In the former complex, the Ru(II) center is in an octahedral environment perched above the P_2N_2 macrocycle having two formally anionic amido donors; in the latter complex, there is only one amido ligand with the other as an amine donor where the proton originates from the cyclometalated triphenylphosphine group. Reaction of the tridentate amidophosphine ligand precursor $[NPN]Li_2(THF)_2$ (where NPN is $PhP(CH_2SiMe_2NPh)_2$) with $[RuCl_2(cod)]_x$ results in the formation of two diastereomeric complexes of the formula $[NPNH]Ru(\eta^3:\eta^2\text{-}C_8H_{11})$, wherein the cyclooctadiene ligand has been deprotonated by the ancillary ligand to generate a cyclooctadienyl unit. These Ru(II) complexes are five-coordinate with a bidentate PN ligand and a dangling amine unit. The diastereomers are in equilibrium, as shown by variable-temperature NMR studies. The fluxional process that interconverts diastereomers involves proton transfer from the dangling amine arm to the amido unit, a process that equilibrates the two ends of the tridentate NPN ligand on the chemical time scale. Deprotonation of the amine arm by $MN(SiMe_3)_2$ generates a series of ruthenate complexes of the formula $[M(THF)]([NPN]Ru(\eta^3:\eta^2\text{-}C_8H_{11}))$, where M = Li or Na. Addition of Me_3SiCl results in the formation of new diastereomers that contain silylated dangling arms, and these diastereomers do not interconvert.

Introduction

In recent years 18-electron ruthenium(II) complexes incorporating phosphine and amine ligands have been employed as precursors for the catalytic asymmetric reduction of prochiral ketone and imine substrates.[1−9] For example, complexes of the type *trans*-$Ru(binap)Cl_2$(diamine) and corresponding hydride derivatives are among the most active catalyst precursors for the hydrogenation of polar substrates and display remarkable chemoselectivity for preferential reduction of polar C=O or C=N functionalities over nonpolar C=C groups.[10]

A widely accepted proposal, labeled the "metal−ligand bifunctional mechanism", involves a cooperative effort between the transition metal hydride and the coordinated amine ligand.[11−17] A critical component of this mechanism is the formation of an intermediate ruthenium amide complex that heterolytically cleaves dihydrogen to regenerate the catalytically active species and, thereby, close the cycle. This last step, the heterolytic cleavage of H_2 by a ruthenium amide ($Ru\text{-}NR_2$) unit, was first demonstrated in our laboratory utilizing the mixed-donor [PNP] (where $[PNP] = N(SiMe_2CH_2PPh)_2$) ligand set.[18]

While a single amide unit is all that is required for the bifunctional mechanism, we were interested in examining the effect of two amido donors coordinated to ruthenium(II). With the late transition elements, anionic amido donors are often quite reactive and can engage in intramolecular proton transfer and migratory insertion.[19−21] Previous work from our laboratory has

* To whom correspondence should be addressed. E-mail: fryzuk@chem.ubc.ca.

(1) Abbel, R.; Abdur-Rashid, K.; Faatz, M.; Hadzovic, A.; Lough Alan, J.; Morris, R. H. *J. Am. Chem. Soc.* **2005**, *127*, 1870.
(2) Abdur-Rashid, K.; Clapham, S. E.; Hadzovic, A.; Harvey, J. N.; Lough, A. J.; Morris, R. H. *J. Am. Chem. Soc.* **2002**, *124*, 15104.
(3) Abdur-Rashid, K.; Fedorkiw, T.; Lough, A. J.; Morris, R. H. *Organometallics* **2004**, *23*, 86.
(4) Mikami, K.; Korenaga, T.; Terada, M.; Ohkuma, T.; Pham, T.; Noyori, R. *Angew. Chem., Int. Ed.* **1999**, *38*, 495.
(5) Noyori, R. *Angew. Chem., Int. Ed.* **2002**, *41*, 2008.
(6) Noyori, R.; Ohkuma, T. *Angew. Chem., Int. Ed.* **2001**, *40*, 40.
(7) Ohkuma, T.; Doucet, H.; Pham, T.; Mikami, K.; Korenaga, T.; Terada, M.; Noyori, R. *J. Am. Chem. Soc.* **1998**, *120*, 1086.
(8) Ohkuma, T.; Hattori, T.; Ooka, H.; Inoue, T.; Noyori, R. *Org. Lett.* **2004**, *6*, 2681.
(9) Ohkuma, T.; Ishii, D.; Takeno, H.; Noyori, R. *J. Am. Chem. Soc.* **2000**, *122*, 6510.
(10) Ohkuma, T.; Ooka, H.; Ikariya, T.; Noyori, R. *J. Am. Chem. Soc.* **1995**, *117*, 10417.
(11) Abdur-Rashid, K.; Faatz, M.; Lough, A. J.; Morris, R. H. *J. Am. Chem. Soc.* **2001**, *123*, 7473.
(12) Abdur-Rashid, K.; Clapham Sean, E.; Hadzovic, A.; Harvey, J. N.; Lough Alan, J.; Morris Robert, H. *J. Am. Chem. Soc.* **2002**, *124*, 15104.
(13) Noyori, R. *Adv. Synth. Catal.* **2003**, *345*, 15.
(14) Noyori, R.; Koizumi, M.; Ishii, D.; Ohkuma, T. *Pure Appl. Chem.* **2001**, *73*, 227.
(15) Yamakawa, M.; Ito, H.; Noyori, R. *J. Am. Chem. Soc.* **2000**, *122*, 1466.
(16) Ohkuma, T.; Ooka, H.; Yamakawa, M.; Ikariya, T.; Noyori, R. *J. Org. Chem.* **1996**, *61*, 4872.
(17) Ohkuma, T.; Ooka, H.; Hashiguchi, S.; Ikariya, T.; Noyori, R. *J. Am. Chem. Soc.* **1995**, *117*, 2675.
(18) Fryzuk, M. D.; Montgomery, C. D.; Rettig, S. J. *Organometallics* **1991**, *10*, 467.

10.1021/om050574i CCC: $30.25
Publication on Web 09/22/2005

Table 1. Selected Bond Lengths and Angles in $[P_2N_2]Ru(\eta^2:\eta^2\text{-}C_8H_{12})$ (1)

atom	atom	distance (Å)
Ru(1)	N(1)/N(1)*	2.223(2)
Ru(1)	P(1)/P(1)*	2.3908(7)
Ru(1)	C(13)/C(13)*	2.200(3)
Ru(1)	C(14)/C(14)*	2.202(3)
C(13)	C(14)	1.386(4)

atom	atom	atom	angle (deg)	atom	atom	atom	angle (deg)
P(1)	Ru(1)	P(1)*	152.18(4)	N(1)	Ru(1)	C(14)*	90.59(10)
N(1)	Ru(1)	N(1)*	92.91(12)	P(1)	Ru(1)	C(13)	83.98(8)
P(1)	Ru(1)	N(1)	75.88(6)	P(1)	Ru(1)	C(13)*	116.39(8)
P(1)	Ru(1)	N(1)*	84.99(6)	P(1)	Ru(1)	C(14)	120.34(8)
N(1)	Ru(1)	C(13)	158.62(10)	P(1)	Ru(1)	C(14)*	80.40(8)
N(1)	Ru(1)	C(13)*	92.40(10)	C(13)	Ru(1)	C(13)*	90.15(16)
N(1)	Ru(1)	C(14)	163.67(9)	C(14)	Ru(1)	C(14)*	90.51(17)

detailed the synthesis of two amidophosphine ligand precursors that each have two amido units attached to one or two phosphine moieties, that is, $[NPN]Li_2(THF)_2$ ([NPN] = $PhP(CH_2SiMe_2NPh)_2$; THF = tetrahydrofuran) and $[P_2N_2]Li_2(Diox)$ ($[P_2N_2]$ = $[PhP(CH_2SiMe_2NSiMe_2CH_2)_2PPh]$; Diox = 1,4-dioxane), respectively.[22,23] In this paper, we report the coordination chemistry of these two multidentate ligands with two Ru(II) precursors. We have already published the reaction of one of these precursor complexes with H_2 and examined its ability to hydrogenate imines and ketones.[24]

Results and Discussion

Synthesis and Characterization of $[P_2N_2]$Ru Complexes. The reaction of colorless $[P_2N_2]Li_2(Diox)$[23] with $[RuCl_2(cod)]_x$ generates a dark yellow-brown solution from which $[P_2N_2]Ru(\eta^2:\eta^2\text{-}C_8H_{12})$ (**1**) can be isolated in 73% yield (eq 1). Compound **1** is the first ruthenium

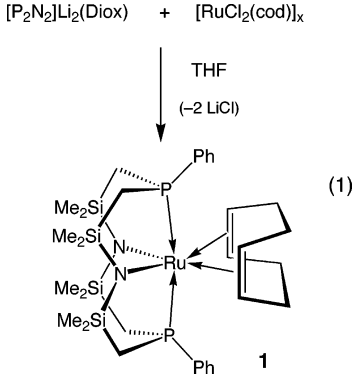

complex of the $[P_2N_2]$ ligand that has been prepared; $[P_2N_2]$ complexes of some early transition metals have previously been investigated.[25,26] Due to the fact that the yellow diamido species **1** is only moderately soluble in hexanes, it can be purified from the more soluble dark colored impurities by rinsing the crude product mixture with hexanes.

The solid-state molecular structure of **1** as determined by a single-crystal X-ray diffraction study is shown in Figure 1, with selected bond lengths and angles highlighted in Table 1. The complex adopts a distorted octahedral geometry in which the amido donors of the $[P_2N_2]$ ligand set and the olefin donors of the cyclooctadiene ligand lie in an equatorial plane. The phosphine ligands occupy the corresponding axial positions with a P(1)−Ru(1)−P(1)* angle of 152.18(4)°. The compound exhibits C_2 symmetry in the solid state.

The smaller N−Ru−N bite angle of 92.91(12)° compared to the larger P−Ru−P bite angle of 152.18(4)° is consistent with the previously observed binding of the $[P_2N_2]$ ligand in which the amide donors are typically *cis* while the phosphines are located approximately *trans* to one another. Similar to $[P_2N_2]$ complexes of the early transition metals,[25,26] the ruthenium center in **1** is perched on, rather than nested in, the macrocycle.

The room-temperature ^1H NMR spectrum of complex **1** in toluene-d_8 is indicative of a C_{2v} symmetric solution structure. For instance, the $[P_2N_2]$ ligand in **1** gives rise to two resonances for the silyl methyl protons at δ 0.4 and 0.5. These correspond to the silyl methyl groups directed to the "top" and "bottom" of the ligand (where top refers to the side of the ligand to which the metal is bound). If the C_2 symmetry evident in the solid-state molecular structure of **1** was maintained in solution, four silyl methyl proton resonances would be expected. In addition, there is a single peak present for the four vinyl protons of the cyclooctadiene ligand and a broad

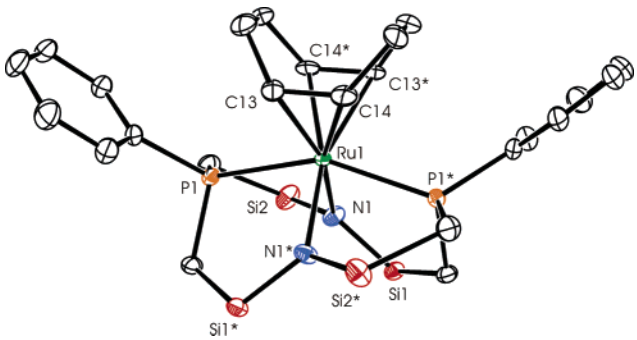

Figure 1. ORTEP representation (thermal ellipsoids shown at 50% probability) of the solid-state molecular structure of $[P_2N_2]Ru(\eta^2:\eta^2\text{-}C_8H_{12})$ (**1**). The silyl methyl groups of the $[P_2N_2]$ ligand have been omitted for clarity.

(19) Fryzuk, M. D.; Montgomery, C. D. *Coord. Chem. Rev.* **1989**, *95*, 1.
(20) Watson, L. A.; Coalter, J. N., III; Ozerov, O.; Pink, M.; Huffman, J. C.; Caulton, K. G. *New J. Chem.* **2003**, *27*, 263.
(21) Fulton, J. R.; Holland, A. W.; Fox, D. J.; Bergman, R. G. *Acc. Chem. Res.* **2002**, *35*, 44.
(22) Fryzuk, M. D.; Johnson, S. A.; Patrick, B. O.; Albinati, A.; Mason, S. A.; Koetzle, T. F. *J. Am. Chem. Soc.* **2001**, *123*, 3690.
(23) Fryzuk, M. D.; Love, J. B.; Rettig, S. J. *J. Chem. Soc., Chem. Commun.* **1996**, 2783.
(24) Fryzuk, M. D.; Petrella, M. J.; Coffin, R. C.; Patrick, B. O. *C. R. Chim.* **2002**, *5*, 451.
(25) Fryzuk, M. D.; Love, J. B.; Rettig, S. J. *Organometallics* **1998**, *17*, 846.
(26) Fryzuk, M. D.; Johnson, S. A.; Rettig, S. J. *Organometallics* **1999**, *18*, 4059.

signal for the eight methylene protons. The $^{13}C\{^1H\}$ NMR spectrum at this same temperature is also consistent with complex **1** exhibiting C_{2v} symmetry in solution. Two resonances for the silyl methyl carbon nuclei are observed and only one peak for the $[P_2N_2]$ methylene carbon nuclei is present; no coupling to the ^{31}P nucleus could be resolved. The cyclooctadiene ligand has a single vinylic carbon resonance at δ 70.0 and a single methylene carbon resonance at δ 25.0.

The high symmetry of complex **1** in solution as evidenced by the ^1H and $^{13}C\{^1H\}$ NMR data is due to the conformationally flexible nature of the $[P_2N_2]$ ligand. The C_{2v} symmetry can be rationalized via a twisting motion of the $[P_2N_2]$ ligand in **1** about the amido nitrogen atoms of the macrocycle that is fast on the NMR time scale.

A variable-temperature ^1H NMR study of complex **1** was undertaken, and the effect of temperature on the vinylic proton resonances of the cyclooctadiene ligand in **1** was monitored. As the temperature is lowered, the singlet at δ 2.80 that is observed at room temperature begins to broaden until decoalescence occurs at 234 K. At the low-temperature limit (198 K) two signals are present at δ 2.6 and 3.0, each integrating to two vinyl protons. Also at 198 K four signals are present for the silyl methyl groups of the $[P_2N_2]$ ligand between δ 0.3 and 0.8. The broad peak for the cyclooctadiene methylene protons collapses to four singlets and the $[P_2N_2]$ methylene protons remain as two peaks. Although the resolution at this temperature was not adequate to provide coupling constants, the features present in the low-temperature limiting spectrum are consistent with C_2 symmetry, as observed in the solid state. A line-shape analysis of the methylene protons of the cyclooctadiene ligand from 212 to 243 K combined with an Arrhenius plot of the resulting rate constants provided an activation barrier of 18.6 $\pm$ 1.6 kcal mol^{-1} for the twisting motion of the $[P_2N_2]$ framework within complex **1** (see Supporting Information).

The reaction of $RuCl_2(PPh_3)_3$ with the $[P_2N_2]$ ligand precursor did not afford the expected diamidodiphosphine ruthenium(II) complex $[P_2N_2]Ru(PPh_3)_2$. Rather, the compound isolated was the product of *ortho*-metalation of one of the triphenylphosphine ligands, $[P_2NNH]Ru(C_6H_4PPh_2)$ (**2**), as shown in eq 2. The propensity for the PPh_3 ligand to *ortho*-metalate is well known not only for complexes of ruthenium(II)[18,27] but for other metals as well.[28,29] Previous studies in the Fryzuk laboratory have shown that the related species [PNP]-RuCl(PPh_3), where [PNP] represents $N(SiMe_2CH_2PPh_2)_2$, suffers a similar fate upon addition of triethylphosphine, resulting in the formation of [PNHP]RuCl-$(C_6H_4PPh_2)$.[18]

Stirring a solution containing an equimolar mixture of $[P_2N_2]Li_2$(Diox) and $RuCl_2(PPh_3)_3$ in toluene results in the formation of an orange-brown solution within 3 h. Removal of LiCl is accomplished by filtration; however, separation of **2** from free triphenylphosphine proved difficult due to the similar solubilities of these two compounds in hydrocarbon solvents. Isolation of **2** was successfully accomplished by the addition of 2 equivalents of anhydrous CuCl; this generates an insoluble "CuCl(PPh_3)" oligomeric complex[30] that is more easily removed by filtration.

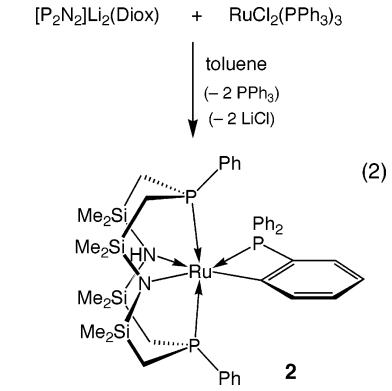

Diagnostic of complex **2** is the $^{31}P\{^1H\}$ NMR spectrum, which shows a doublet (at δ 25.8) and a triplet (at δ −11.8) for the ancillary phosphine donors of the $[P_2NNH]$ ligand set and the $(C_6H_4)PPh_2$ ligand, respectively ($^2J_{PP}$ = 31 Hz). These signals integrate in the ratio 2:1. An upfield shift for the ^{31}P nucleus of the (C_6H_4)-PPh_2 ligand has been observed in other complexes that incorporate an *ortho*-metalated triphenylphosphine ligand.[31] The equivalency of the phosphorus centers in the $[P_2NNH]$ ligand is consistent with the proposed structure, which has C_s symmetry.

The room-temperature 500 MHz ^1H NMR data are also consistent with the proposed structure of complex **2** shown in eq 2. Four resonances for the silylmethyl groups of the $[P_2NNH]$ ligand set are observed between δ 0.40 and 0.60 in accordance with a mirror plane of symmetry contained within the equatorial plane of the octahedral coordination geometry of **2**. The ligand methylene protons give rise to two sets of overlapping resonances consisting of a second-order AA′BX pattern. A singlet at δ 2.8 has been ascribed to the amino proton (N-*H*). The aromatic protons of the *ortho*-metalated triphenylphosphine and $[P_2N_2]$ phosphorus phenyl substituents occur as overlapping resonances between δ 6.5 and 8.2.

Single crystals of $[P_2NNH]Ru(C_6H_4PPPh_2)$ (**2**) suitable for an X-ray diffraction study were grown by the slow evaporation of a saturated pentane solution. The solid-state molecular structure of **2** as determined by X-ray crystallography is shown in Figure 2, with selected bond lengths and bond angles detailed in Table 2. Complex **2** crystallizes with two crystallographically distinct but structurally related molecules in the asymmetric unit, in addition to one molecule of *n*-pentane. The following structural discussion will be concerned with only one of the molecules for the sake of brevity.

The geometry of complex **2** was found to be distorted octahedral with the two phosphine donors of the $[P_2NNH]$ ligand occupying the axial positions; these are pinched back from an ideal *trans* disposition giving a

(27) Pez, G. P.; Grey, R. A.; Corsi, J. *J. Am. Chem. Soc.* **1981**, *103*, 7528.
(28) McKinney, R. J.; Knobler, C. B.; Huie, B. T.; Kaesz, H. D. *J. Am. Chem. Soc.* **1977**, *99*, 2988.
(29) Jones, W. D.; Rosini, G. P.; Maguire, J. P. *Organometallics* **1999**, *18*, 1754.
(30) Cotton, F. A.; Wilkinson, G. *Advanced Inorganic Chemistry: A Comprehensive Text*, 4th ed.; John Wiley and Sons: New York, 1980; pp 804−805.
(31) Cole-Hamilton, D. J.; Wilkinson, G. *J. Chem. Soc., Dalton Trans.* **1977**, 797.

Table 2. Selected Bond Lengths and Bond Angles in [P_2NNH]Ru($C_6H_4PPh_2$) (2)

atom	atom	distance (Å)	atom	atom	distance (Å)
Ru(1)	C(26)	2.034(5)	Ru(1)	P(1)	2.3565(13)
Ru(1)	N(2)	2.260(4)	Ru(1)	N(1)	2.414(4)
Ru(1)	P(3)	2.2989(13)	N(1)	H(101)	0.73(6)
Ru(1)	P(2)	2.3248(13)	N(2)	H(101)	2.404

atom	atom	atom	angle (deg)	atom	atom	atom	angle (deg)
C(26)	Ru(1)	N(2)	99.66(18)	P(3)	Ru(1)	P(1)	93.02(5)
C(26)	Ru(1)	P(3)	68.39(14)	P(2)	Ru(1)	P(1)	168.67(5)
N(2)	Ru(1)	P(3)	167.65(12)	C(26)	Ru(1)	N(1)	178.48(18)
C(26)	Ru(1)	P(2)	93.96(14)	N(2)	Ru(1)	N(1)	79.33(17)
N(2)	Ru(1)	P(2)	86.15(11)	P(3)	Ru(1)	N(1)	112.55(13)
P(3)	Ru(1)	P(2)	97.51(5)	P(2)	Ru(1)	N(1)	87.12(11)
C(26)	Ru(1)	P(1)	93.80(14)	P(1)	Ru(1)	N(1)	84.99(11)
N(2)	Ru(1)	P(1)	84.41(11)	N(1)	H(101)	N(2)	137.72

P(1)−Ru(1)−P(2) angle of 168.67(5)°. The *ortho*-metalated triphenylphosphine ligand as well as the amide and amine ligands all lie in the plane of the octahedron with a combined equatorial angle of 359.93°. The N(1)−Ru(1)−N(2) bond angle of 79.33(17)° is quite small in comparison to complex **1**, which has a N−Ru−N bond angle of approximately 92°. It is likely that this smaller bond angle in **2** is a consequence of an intramolecular hydrogen-bonding interaction between the amino proton and the amido nitrogen atom (vide infra). The ruthenium−amido bond length, Ru(1)−N(2), of 2.260(4) Å is similar to that found in **1**, while the ruthenium−amine bond length, Ru(1)−N(1), is longer at 2.414(4) Å as expected; this latter bond distance is longer than that found in related systems.[18,20] As expected, the amido nitrogen N(2) is essentially planar, with the sum of the angles being 358.1°, while the geometry around the amine nitrogen N(1) is distorted slightly away from planar, with the sum of the angles (excluding the H atom) being 350.9° (Si(2)−N(1)−Si(1), 127.2(3)°; Si(2)−N(1)−Ru(1), 109.4(2)°; Si(1)−N(1)−Ru(1), 114.3(2)°).

The Ru−P bond distances (2.3248(13) and 2.3565(13) Å) for the [P_2NNH] ligand of complex **2** are slightly elongated compared to P(3) of the metalated triphenylphosphine (2.2989(13) Å). Presumably this structural feature is due to the high *trans* influence of phosphines relative to that of amides. This difference, however, is not as significant as that observed in the isoelectronic species [PNHP]RuCl($C_6H_4PPh_2$).[18] In this complex, the phosphine donors of the tridentate ligand are displaced 2.3945 Å on average from the Ru(II) center, whereas the Ru−P distance for the metalated triphenylphosphine ligand is 2.2545 Å. These distances are comparable to those found in $RuCl_2(PPh_3)_3$,[32] in which the two mutually *trans* triphenylphosphine ligands exhibit Ru−P distances of 2.374(6) and 2.388(7) Å, while the remaining phosphine (*trans* to an open site) is located 2.230(8) Å from the metal. The shorter Ru−P distances for the phosphine donors of the [P_2NNH] ligand in **2** may be the result of a "macrocyclic effect".[33] The longer Ru(1)−P(3) distance in complex **2**, on the other hand, may be a consequence of minimizing steric interactions with the [P_2NNH] ligand set.

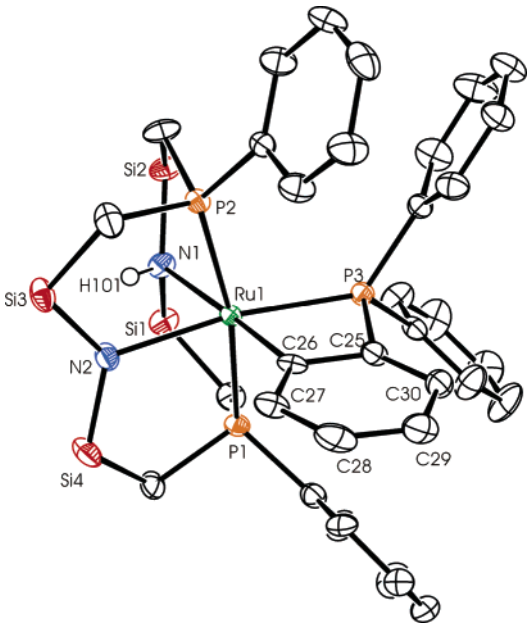

Figure 2. Solid-state molecular structure (ORTEP representation, 50% thermal ellipsoid probability) of [P_2NNH]-Ru($C_6H_4PPh_2$) (**2**) as determined by X-ray crystallography. The silylmethyl groups of the [P_2NNH] ligand have been omitted for clarity.

Structural features of the four-membered ring of the metallacycle are typical of other such rings found in the literature. For instance, the C−Ru−P angle of 68.39(14)° measured in **2** is similar to that found in the ruthenate complex K[$RuH_2(C_6H_4PPh_2)(PPh_3)_2$][27] (67.6(3)°), as well as the related species [PNHP]RuCl($C_6H_4PPh_2$) (68.24(8)°).[18] In the ruthenate complex, the Ru−C distance is 2.098(11) Å, whereas in the tridentate [PNHP] complex it is observed to be 2.054(3) Å. In **2**, a slightly shorter Ru−C distance of 2.034(5) Å was found. This trend in bond distances is in accordance with the *trans* influence differences between PPh_3, Cl, and amine donors[34] in the respective complexes. The ruthenium−amine bond length in complex **2** is likewise lengthened (2.414(4) Å) by the high *trans* influence of the *ortho*-metalated aryl group.

An interesting feature evident in the solid-state molecular structure of complex **2** is the presence of a hydrogen bond between the amine proton (H(101)) and the amido nitrogen (N(2)). A similar bonding interaction was also evident between the amine and chloride ligands in the complex [PNHP]RuCl($C_6H_4PPh_2$), as well as in other complexes of rhodium and iridium that also

(32) Hoffman, P. R.; Caulton, K. G. *J. Am. Chem. Soc.* **1975**, *97*, 4221.

(33) Cotton, F. A.; Wilkinson, G.; Murillo, C. A.; Bochmann, M. *Advanced Inorganic Chemistry: A Comprehensive Text*, 6th ed.; John Wiley and Sons: Toronto, 1999; pp 29−30.

(34) Miessler, G. L.; Tarr, D. A. *Inorganic Chemistry*, 3rd ed.; Prentice Hall: Upper Saddle River, NJ, 2004; p 439.

Scheme 1

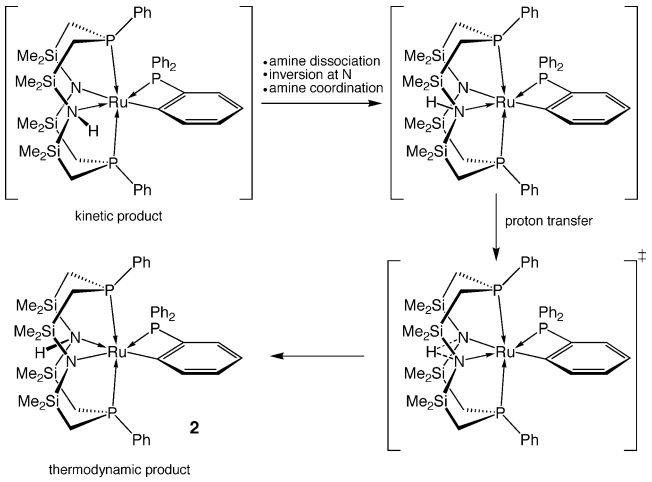

incorporate this tridentate ligand system.[35] The NH···N distance of 2.404 Å in complex **2** is shorter than the expected van der Waals contact distance of 2.7 Å between these two nuclei.[36] Also indicative of the presence of a bonding interaction between the hydrogen and amido nitrogen atom is the fact that the amine hydrogen lies nearly in the plane of N(1), N(2), and Ru(1) illustrated by the Ru(1)−N(1)−H(101)−N(2) torsion angle of −15.1°, thus minimizing the NH···N separation.

The mechanism of the observed *ortho*-metalation to form **2** is unknown. However, one might have expected that transfer of the *ortho*-hydrogen atom to the amido donor would result in *cis*-disposed amine and σ-aryl ligands in the product. In fact, the solid-state data show that the amine ligand is located *trans* to the *ortho*-metalated carbon atom. One rationalization for this may be that the reaction of the $[P_2N_2]$ ligand with $RuCl_2(PPh_3)_3$ is not kinetically controlled and that the formation of complex **2** proceeds under thermodynamic control. The position of the donors in the equatorial plane may be governed by electronics and arranged according to the relative *trans* influences of phosphine, amine, aryl, and amide ligands. The known *trans* influence decreases in the order $PPh_3 > C_6H_5 >$ amine,[34] suggesting that the amido ligand in **2** may exhibit the weakest *trans* influence. Scheme 1 depicts a plausible reaction pathway for the formation of the isolated species **2**. Activation of the *ortho* C−H bond of the PPh_3 would result in a *cis* disposition of the N−H and the σ-bound aryl group in the kinetic product. It is speculated that the amine donor in the kinetic product dissociates, undergoes inversion at nitrogen, and recoordinates, allowing for an intramolecular hydrogen-bonding interaction with the coordinated amido ligand. Subsequent transfer of the amino proton to the amide nitrogen atom generates the observed complex **2**. A similar rearrangement was proposed to occur upon *ortho*-metalation in the complex [PNHP]RuCl(C_6H_4-PPh_2).[18]

Synthesis, Characterization, and Reactivity of *exo*- and *endo*-[NPNH]Ru(η^3:η^2-C_8H_{11}) (*exo*-3 and *endo*-3). As already discussed, the incorporation of the macrocyclic $[P_2N_2]$ ligand onto Ru(II) via reaction with $[RuCl_2(cod)]_x$ generates the species $[P_2N_2]Ru(\eta^2$:η^2-$C_8H_{12})$ (**1**). Thus it was anticipated that the outcome of the reaction between the tridentate [NPN] ligand precursor $[NPN]Li_2(THF)_2$ (where [NPN] is $PhP(CH_2SiMe_2NPh)_2$) with $[RuCl_2(cod)]_x$ would be the formation of the diamidophosphine complex $[NPN]Ru(\eta^2$:η^2-$C_8H_{12})$, as shown in eq 3. That this was not the isolated product from this reaction was immediately apparent upon inspection of the room-temperature ^1H NMR spectrum (Figure 3). Just the sheer number of peaks present implied the existence of more than one species (each of low symmetry) in solution, and furthermore, the broadened resonances were indicative of a fluxional process occurring in solution. The ^1H NMR spectra at 298 and 245 K are shown in Figure 3. However, elemental analysis of the red crystalline solid that was isolated from this reaction is consistent with the formulation of the expected product, $[NPN]Ru(\eta^2$:η^2-$C_8H_{12})$, suggesting that the isolated products were structurally related isomers of this species.

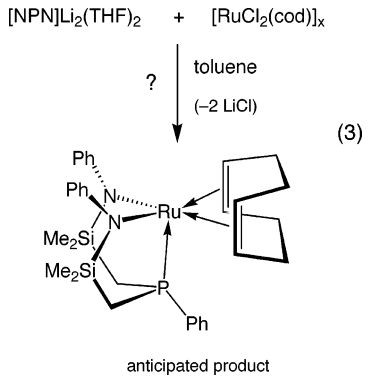

(3)

As portrayed in eq 4, the products that are formed in the reaction between the [NPN] ligand precursor and $[RuCl_2(cod)]_x$ are a pair of diastereomers. Transfer of an allylic C-H atom of the cyclooctadiene ligand to one of the amido donors of the [NPN] ligand occurs, generating a mixture of the two species *exo*- and *endo*-[NPNH]-Ru(η^3: η^2-C_8H_{11}) (*exo*-**3** and *endo*-**3**, respectively). The activation of an allylic C−H bond of a coordinated cyclooctadiene moiety resulting in the formation of a

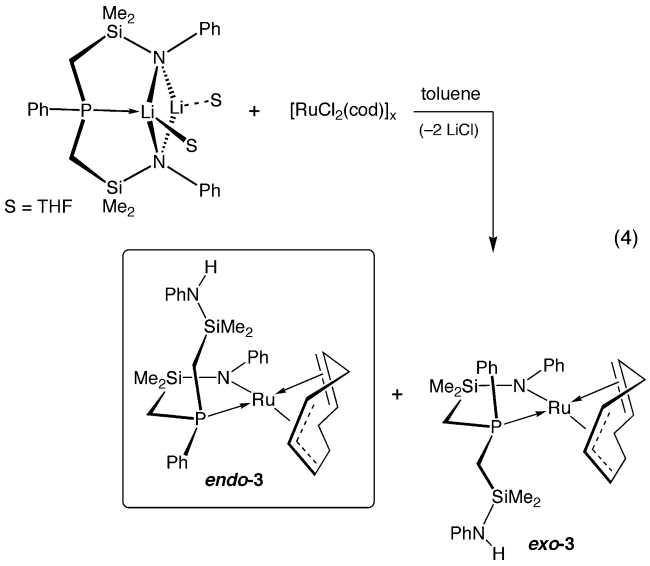

(4)

(35) Fryzuk, M. D.; MacNeil, P. A.; Rettig, S. J. *J. Am. Chem. Soc.* **1987**, *109*, 2803.

(36) Joesten, M. D.; Schaad, L. J. *Hydrogen Bonding*; Marcel Dekker: New York, 1974.

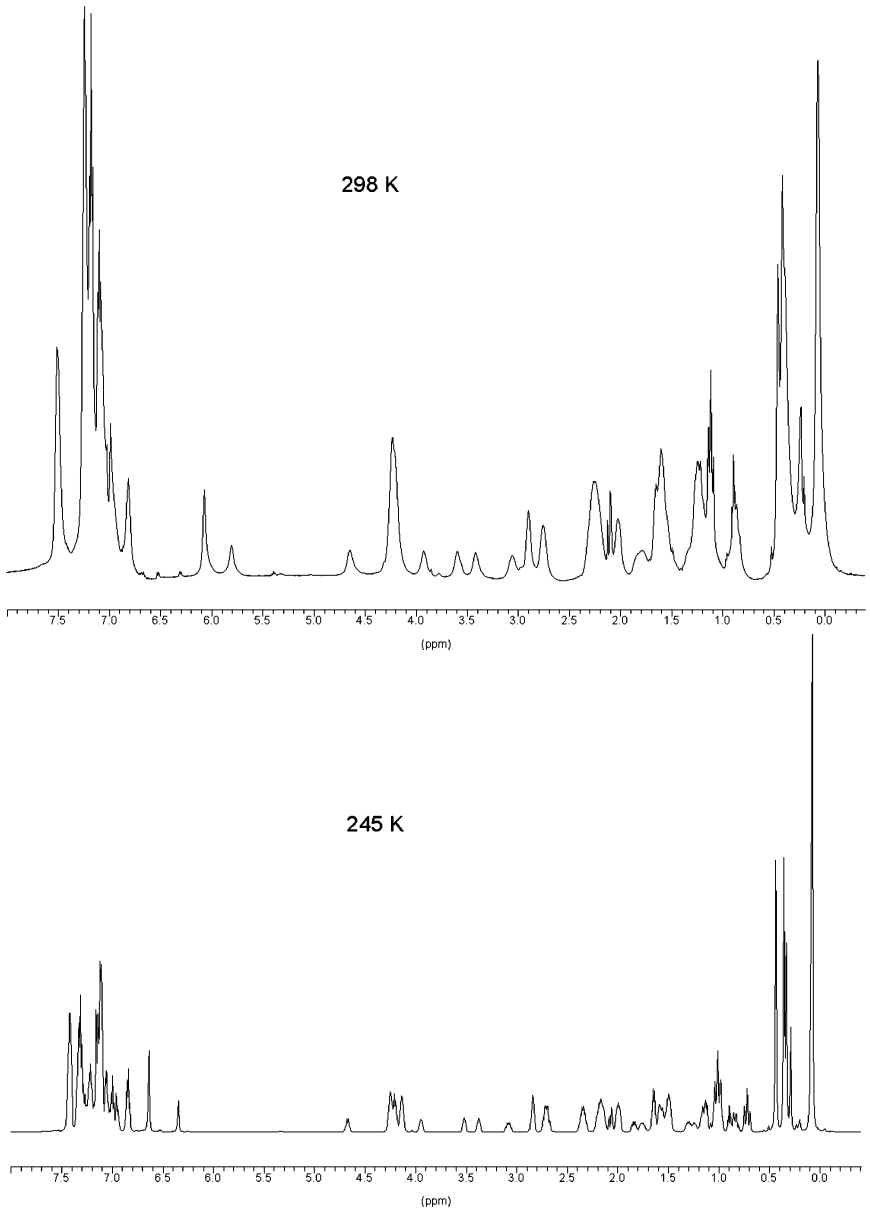

Figure 3. 500 MHz ^{1}H NMR spectrum of the mixture of complexes **3** in toluene-d_8 at 298 K (upper spectrum) and 245 K (lower spectrum).

cyclooctadienyl ruthenium(II) complex has previously been reported.[37,38] The terms "*exo*" and "*endo*" are used to distinguish the two diastereomers, and they refer to the orientation of the amino sidearm of the [NPNH] ligand set with respect to the methylene unit bridging the olefin and allyl donor groups of the cyclooctadienyl ligand. In the *endo* diastereomer the pendant amino ligand and the bridging methylene unit are oriented toward the same "side" of the metal, whereas in the *exo* isomer, the amino ligand is positioned to the opposite face of the metal and points away from the bridging methylene unit.

The identification and characterization of the diastereomers *exo*-**3** and *endo*-**3**, as well as an understanding of the dynamic behavior of these two species in solution, proved to be challenging. Techniques including X-ray crystallography and variable-temperature one- and two-dimensional NMR spectroscopy (^{1}H, ^{13}C{^{1}H}, and ^{31}P{^{1}H}) in addition to reactivity studies all provided valuable clues about this system.

The solid-state structural identification of the diastereomer *endo*-**3** provided the first insight into the details of the reaction of the [NPN] ligand precursor with $[RuCl_2(cod)]_x$. The solid-state molecular structure is shown in Figure 4; pertinent bond lengths and angles can be found in Table 3. Transfer of an allylic C-H atom of the cyclooctadiene ligand to an amido nitrogen atom is clearly evident from the solid-state molecular structure, which shows the η^3-allyl, η^2-olefin coordination mode adopted by the cyclooctadienyl ligand. The protonated sidearm of the [NPNH] ligand is also apparent, and it does not coordinate to the metal center. The amino proton (H43) was located and refined isotropically. The complex exhibits a five-coordinate, distorted trigonal bipyramidal geometry at ruthenium (with the allyl donor occupying two coordination sites and the

(37) Ashworth, T. V.; Chalmers, A. A.; Liles, D. C.; Meintjies, E.; Singleton, E. *Organometallics* **1987**, *6*, 1543.
(38) Wiles, J. A.; Lee, C. E.; McDonald, R.; Bergens, S. H. *Organometallics* **1996**, *15*, 3782.

Table 3. Selected Bond Lengths and Angles in *endo*-[NPNH]Ru(η^3: η^2-C_8H_{11}) (*endo*-3)

atom	atom	distance (Å)	atom	atom	distance (Å)
Ru(1)	N(1)	2.019(2)	C(29)	C(30)	1.408(4)
Ru(1)	P(1)	2.3024(6)	C(30)	C(31)	1.411(4)
Ru(1)	C(25)	2.300(3)	N(1)	C(7)	1.430(3)
Ru(1)	C(26)	2.332(2)	N(2)	C(19)	1.392(3)
Ru(1)	C(29)	2.187(2)	N(1)	Si(1)	1.734(2)
Ru(1)	C(30)	2.169(2)	N(2)	Si(2)	1.727(2)
Ru(1)	C(31)	2.195(2)	N(1)	H(43)	3.419
C(25)	C(26)	1.354(4)			

atom	atom	atom	angle (deg)	atom	atom	atom	angle (deg)
P(1)	Ru(1)	N(1)	87.32(6)	N(1)	Ru(1)	C(29)	147.35(9)
P(1)	Ru(1)	C(25)	163.35(7)	N(1)	Ru(1)	C(30)	170.65(9)
P(1)	Ru(1)	C(26)	162.61(7)	N(1)	Ru(1)	C(31)	142.72(9)
P(1)	Ru(1)	C(29)	95.22(7)	Ru(1)	N(1)	Si(1)	124.3(1)
P(1)	Ru(1)	C(30)	83.98(7)	Ru(1)	N(1)	C(7)	123.6(2)
P(1)	Ru(1)	C(31)	103.09(7)	Si(1)	N(1)	C(7)	112.2(2)
N(1)	Ru(1)	C(25)	97.09(9)	C(29)	Ru(1)	C(31)	68.2(1)
N(1)	Ru(1)	C(26)	90.06(9)				

olefin donor one coordination site). Within the trigonal bipyramid, the amide and the allyl moieties lie within the trigonal plane, while the phosphine and olefin ligands occupy the axial positions. The P(1)−Ru(1)−C(25) and P(1)−Ru(1)−C(26) bond angles are 163.35(7)° and 162.61(7)°, respectively, indicating a nearly *trans* disposition between the phosphine and olefin donor groups. The allyl moiety of the cyclooctadienyl ligand is symmetrically bound to ruthenium with an average Ru−C_{allyl} bond distance of 2.184 Å.

Although **3** may be considered an unsaturated, 16-electron species, the presence of the π-donating amido ligand can also result in a formal 18-electron configuration at the metal center. An indication of a π-bonding interaction can be portrayed structurally by a short metal−nitrogen bond distance as well as a trigonal planar coordination geometry at the amido nitrogen atom.[19] In the case of *endo*-**3** the ruthenium amide (Ru(1)−N(1)) bond length is 2.019(2) Å. In contrast, the coordinatively saturated species [P_2N_2]Ru(η^2:η^2-C_8H_{12}) (**1**) has a Ru−N bond length of 2.223(2) Å. The six-coordinate complexes *cis*-Ru(H)(PMe_3)$_4$(NHPh)[39] and Ru(η^6-C_6Me_6)(PMe_3)(Ph)(NHPh)[40] bearing the anilido ligand have ruthenium to nitrogen distances of 2.160(6) and 2.121(3) Å, respectively. The shorter Ru−N bond length in the five-coordinate *endo*-**3** can be attributed to delocalization of the amido nitrogen lone pair to a vacant metal d-orbital. Also consistent with the existence of a π-bonding interaction is the planar, sp^2-hydridized geometry displayed by the amido nitrogen atom (sum of angles = 360°); planarity of the amido unit necessarily occurs to maximize π-bonding with the metal center. This planarity, however, could also arise from similar π-interactions existing between the amide nitrogen atom and the neighboring silicon atom or phenyl ring. The bond distance (1.430(3) Å) from the amido nitrogen (N(1)) to the phenyl *ipso* carbon (C(7)) of the amido moiety is longer than that of aniline (1.398 Å), suggesting minimal π-delocalization into the amido aromatic ring in complex *endo*-**3**. In an earlier report, an inverse correlation between Ru−N and N−C_{ipso} bond distances in ruthenium(II) phenyl amido systems had been noted.[41]

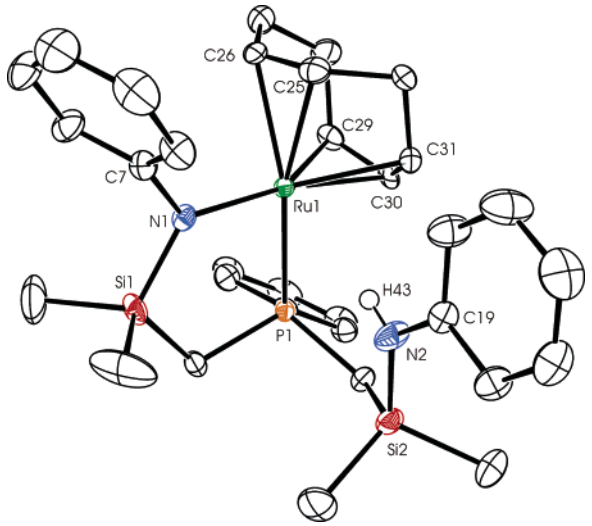

Figure 4. Solid-state molecular structure (ORTEP depiction shown at 50% thermal ellipsoid probability) of *endo*-[NPNH]Ru(η^3: η^2-C_8H_{11}) (*endo*-**3**) as determined by X-ray diffraction. The amino proton (H43) was refined isotropically.

Theoretical calculations[42,43] have shown that a diamagnetic d^6 ML_5 complex distorts away from the Jahn−Teller active trigonal bipyramidal structure to generate either a square pyramid or a distorted trigonal bipyramid type geometry. These two extreme geometries were found to be very close in energy, and the preference for one over the other comes from a subtle balance of the σ- and π-properties of the ligands. When one of the ligands is a π-donor, a distorted trigonal bipyramidal geometry is observed[44−47] with this ligand located opposite the acute angle in the equatorial plane of the

(39) Hartwig, J. F.; Andersen, R. A.; Bergman, R. G. *Organometallics* **1991**, *10*, 1875.
(40) Boncella, J. M.; Eve, T. M.; Rickman, B.; Abboud, K. A. *Polyhedron* **1998**, *17*, 725.
(41) Jayaprakash, K. N.; Gunnoe, T. B.; Boyle, P. D. *Inorg. Chem.* **2001**, *40*, 6481.
(42) Rachidi, I. E. I.; Eisenstein, O.; Jean, Y. *New J. Chem.* **1990**, *14*, 671.
(43) Riehl, J. F.; Jean, Y.; Eisenstein, O.; Pelissier, M. *Organometallics* **1992**, *11*, 729.
(44) Johnson, T. J.; Folting, K.; Streib, W. E.; Martin, J. D.; Huffman, J. C.; Jackson, S. A.; Eisenstein, O.; Caulton, K. G. *Inorg. Chem.* **1995**, *34*, 488.
(45) Bickford, C. C.; Johnson, T. J.; Davidson, E. R.; Caulton, K. G. *Inorg. Chem.* **1994**, *33*, 1080.
(46) Poulton, J. T.; Sigalas, M. P.; Folting, K.; Streib, W. E.; Eisenstein, O.; Caulton, K. G. *Inorg. Chem.* **1994**, *33*, 1476.

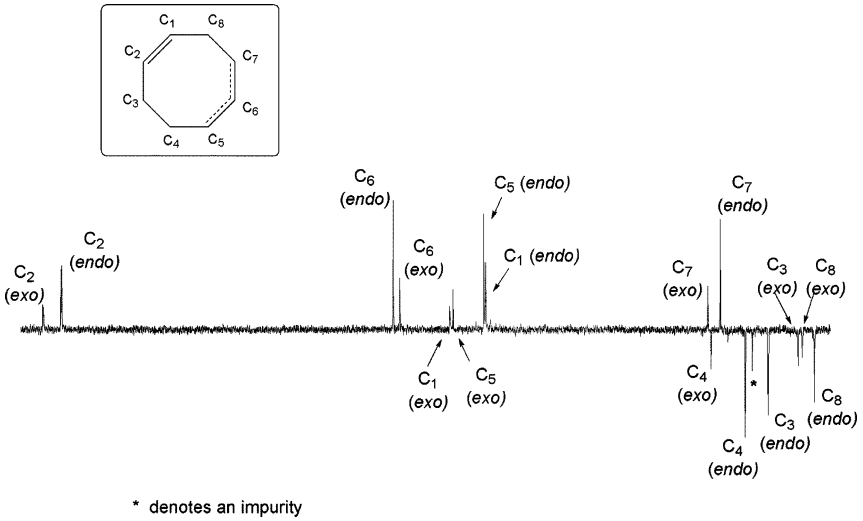

Figure 5. *J*-modulated $^{13}C\{^1H\}$ NMR spectrum for *endo*-**3** and *exo*-**3** obtained at 245 K in toluene-d_8 highlighting the cyclooctadienyl carbon resonances. The *C*H resonances point up and the *C*H_2 resonances point down. The spectral range indicated is from δ 110 for C_2 (*exo*) to δ 25 for C_8 (*endo*).

molecule. Such a geometry permits the formation of a partial double bond between an empty metal d-orbital and the lone pair of the π-donor, which is manifested as a shortening in the M−X bond and, in the case of a single-face π-donor, a preferred orientation to maximize orbital overlap. No such π-interaction can occur in the square pyramidal structure since all of the appropriate symmetry-adapted d-orbitals are filled.

The observed geometry of *endo*-**3** in the solid state coincides well with the theoretical predictions and on the basis of orbital symmetry allows for amide-to-ruthenium multiple bonding to take place. The P(1)−Ru(1)−N(1)−Si(1) dihedral angle of −5.8(1)° indicates that the plane of the amide donor is perpendicular to the equatorial plane of the molecule, and this allows for maximal overlap of the filled amido lone pair orbital (p_y) with the empty d_{xy} metal orbital. Complex **3** can therefore be regarded as a "π-stabilized" unsaturated complex.

As already mentioned, the room-temperature ^1H NMR spectrum of **3** indicates the presence of (at least) two species in solution, and furthermore, the number of resonances observed suggests that these complexes are of low symmetry. The characterization of *endo*-**3** in the solid state shows that it is chiral, exhibiting C_1 symmetry. By examination of the spectra in more detail, it was determined that there were two species in solution, in equilibrium with each other and displaying similar types of environments for the cyclooctadienyl resonances and the ancillary ligand. The room-temperature ^1H NMR spectrum of a bulk sample of **3** consists of many broadened resonances, which hampered peak assignments (see Figure 3). The $^{31}P\{^1H\}$ NMR spectrum at the same temperature contains one peak at δ 33.0. Cooling the sample, however, results in two singlets in the $^{31}P\{^1H\}$ NMR spectrum in the ratio 2:1, establishing the presence of two species (one major and one minor) in solution. It was not possible to determine which diastereomer is the major or minor species; therefore, in the following discussion concerning the variable-temperature NMR studies it is assumed that *endo*-**3** is the major isomer in solution.

Interestingly, identical NMR spectra (^1H and $^{31}P\{^1H\}$) are obtained whether a single crystal of *endo*-**3** is employed for the NMR investigations or a bulk powdered sample. This suggests that a dynamic equilibrium exists between the two species in solution. At 245 K the fluxional process responsible for the interconversion of the two species is slow enough to allow for the identification of *endo*-**3** and *exo*-**3** as the two complexes in solution. Full characterization of these two isomers was based on low-temperature ^1H, $^{31}P\{^1H\}$, and $^{13}C\{^1H\}$ NMR data. In addition, two-dimensional homo- and heteronuclear correlation experiments allowed for the complete assignment of the resonances attributed to both of the diastereomers. A collection of the ^1H and ^{13}C assignments for the cyclooctadienyl ligand of isomers *endo*-**3** and *exo*-**3** is given in the Supporting Information, together with data for other complexes containing this ligand. The labeling convention used for assignment of NMR peaks corresponding to the cyclooctadienyl ligand that will be used in the following discussion is shown in the Experimental Section.

The *J*-modulated $^{13}C\{^1H\}$ NMR spectrum obtained at 245 K (shown in Figure 5) identifies the presence of 10 CH and six CH_2 resonances for the cyclooctadienyl ligand, consistent with an η^3-allyl, η^2-olefin coordination mode for each isomer. Complex *endo*-**3** contains two doublets at δ 108.1 ($^2J_{PC}$ = 10.5 Hz) and 61.4 ($^2J_{PC}$ = 6.5 Hz) in the $^{13}C\{^1H\}$ NMR spectrum that have been ascribed as the olefinic bound carbon atoms C_2 and C_1, respectively; these show a two-bond coupling with the *trans*-located phosphine donor. The allyl carbon resonances occur at δ 71.6 (C_6), 61.6 (C_5), and 35.6 (C_7). For these latter peaks no scalar coupling to the ^{31}P nucleus could be resolved; a much smaller coupling would be expected due to the *cis* orientation between these two donor groups. These data agree with the solid-state structure, which shows that the olefin and phosphine donors are *trans*-disposed to one another.

The 500 MHz ^1H NMR spectrum of *endo*-**3** shows four silyl methyl and four methylene proton resonances of the [NPNH] ligand, indicating that the asymmetry of

(47) Fryzuk, M. D.; MacNeil, P. A.; Rettig, S. J. *Organometallics* **1986**, *5*, 2469.

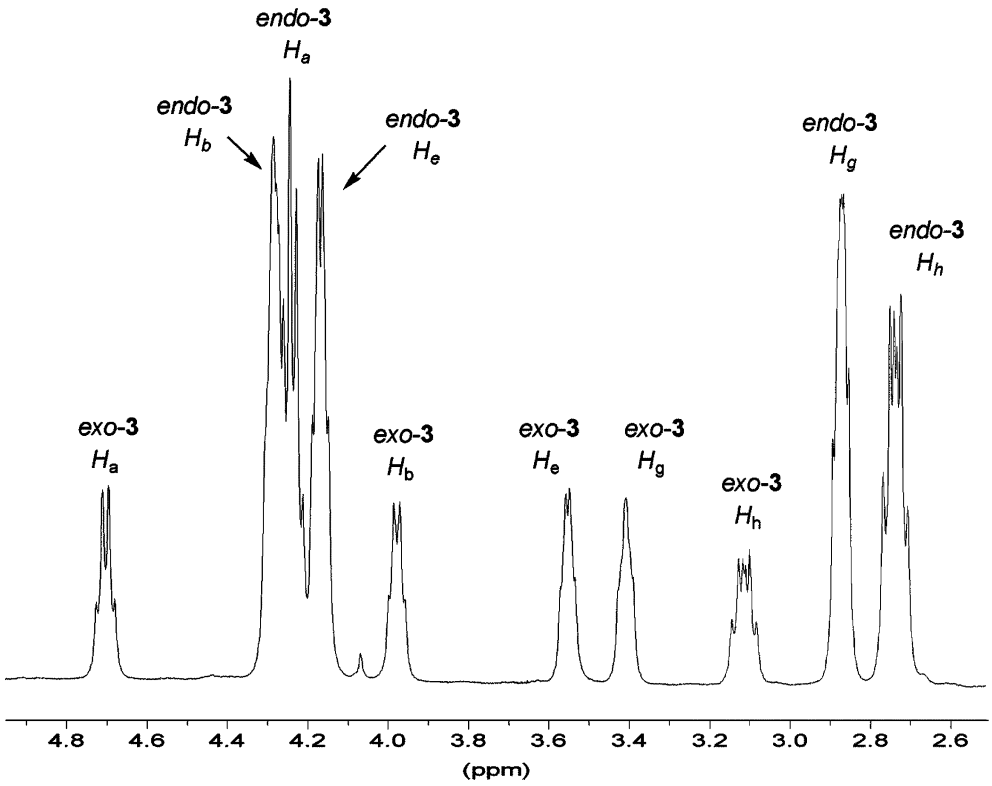

Figure 6. Region of the 500 MHz $^1H\{^{31}P\}$ NMR spectrum of isomers *endo*-**3** and *exo*-**3** highlighting the downfield shifted cyclooctadienyl proton resonances at 245 K in toluene-d_8.

the complex is maintained in solution. In addition, all 11 cyclooctadienyl protons are inequivalent and give rise to 11 coupled resonances. The olefinic protons are shifted furthest downfield at δ 4.25 (H_b) and 4.23 (H_a), respectively. The terminal allyl proton resonances are found at δ 4.20 (H_e) and 2.85 (H_g), whereas the central allyl proton (H_f) is significantly upfield shifted at δ 1.64. The protons of the methylene unit bridging the olefin and allyl groups (H_h and H_h') are observed as multiplets at δ 2.70 and 2.00. The remaining methylene proton environments of the cyclooctadienyl ligand are located at δ 2.63 (H_c), 1.58 (H_c'), 2.18 (H_d), and 1.50 (H_d'). The two-dimensional $^1H-^1H$ COSY and $^1H-^{13}C$ HMQC data aided in the assignment of the cyclooctadienyl proton environments. The amino proton of the dissociated sidearm of the [NPNH] ligand occurs as a singlet at δ 6.63.

Inspection of the ^{13}C resonances for the cyclooctadienyl carbon nuclei of the minor isomer shows that they are only slightly shifted with respect to *endo*-**3**, suggesting a very similar coordination mode adopted by this ligand. Furthermore, two doublets at δ 110.0 ($^2J_{PC}$ = 11.3 Hz) and 65.3 ($^2J_{PC}$ = 5.8 Hz) indicate that the phosphine donor is located *trans* to the olefin moiety, a feature that was also evident in the $^{13}C\{^1H\}$ NMR spectrum of *endo*-**3**. These data are consistent with *exo*-**3** as the second species in solution.

The ^1H NMR data also support the formulation of the second species in solution as diastereomer *exo*-**3**. Figure 6 shows a region of the 500 MHz $^1H\{^{31}P\}$ NMR spectrum highlighting the downfield-shifted cyclooctadienyl resonances for both diastereomers. In addition to exhibiting a similar trend in the chemical shift of the proton environments, both *endo*-**3** and *exo*-**3** display similar coupling patterns, which is consistent with the same coordination mode adopted by the cyclooctadienyl ligand in both species. For *exo*-**3**, the olefinic protons exist furthest downfield at δ 4.68 (H_a) and 3.92 (H_b) with the two terminal allyl protons at δ 3.50 (H_e) and 3.37 (H_g). Although the central allyl proton (H_f) is obscured by neighboring peaks, its presence at δ 1.50 was confirmed by $^1H-^1H$ and $^1H-^{13}C$ correlation experiments. The significant upfield shift of this proton also occurs for isomer *endo*-**3**. To further assist in the characterization of isomer *exo*-**3**, a simulation of the spin system of the cyclooctadienyl proton environments was performed. The calculated coupling constants, tabulated in the Supporting Information, are similar to those obtained for other complexes known to contain a η^3,η^2-cyclooctadienyl ligand bound to ruthenium(II).[37] An asymmetric solution structure for *exo*-**3** is also apparent from the four silyl methyl and four methylene proton environments of the [NPNH] ligand set. The amino proton occurs at δ 6.35, shifted 0.28 ppm upfield from the amino proton of *endo*-**3**.

Analysis of the variable-temperature ^1H NMR data confirmed the existence of an equilibrium between the species *endo*-**3** and *exo*-**3** in solution. Integration of the amino proton resonance for each of the diastereomers at various temperatures gave relative concentrations of the two isomers and allowed for the evaluation of the equilibrium constants according to K = [*endo*-**3**]/[*exo*[**3**]. A van't Hoff plot permitted the determination of the following thermodynamic parameters for the equilibrium process: $\Delta H° = 0.93 \pm 0.10$ kcal mol^{-1} and $\Delta S° = 1.62 \pm 0.20$ eu (see Supporting Information).

Figure 7 shows the N-*H* region of the two-dimensional EXSY spectrum obtained at room temperature (500 MHz, t_{mix} = 400 ms) for the mixture of *endo*-**3** and *exo*-**3** in toluene-d_8. A positively phased cross-peak between

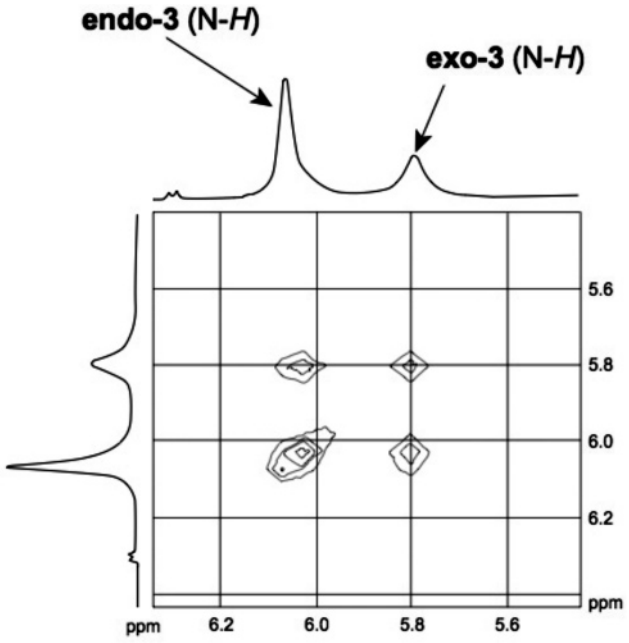

Figure 7. N-*H* region of the 2-D EXSY spectrum for the mixture of *endo*-**3** and *exo*-**3**. Obtained at 298 K in toluene-d_8, 500 MHz, and a mixing time of 0.4 s.

sites in a 2D-EXSY spectrum indicates that these nuclei are in chemical exchange, providing further evidence for the dynamic equilibrium that exists in solution. No cross-peaks were observed between the amino protons and any of the cyclooctadienyl proton resonances, indicating that the N-*H* proton does not get incorporated into the cyclooctadienyl ligand. Cross-peaks were also observed for resonances associated with the cyclooctadienyl ligand; however, due to the fact that these peaks were broadened and overlapping at 298 K, they could not be assigned to specific proton environments. The [NPNH] silyl methyl and methylene resonances between isomers also gave rise to positively phased cross-peaks as would be expected.

The interconversion of the two diastereomers *endo*-**3** and *exo*-**3** requires inversion of chirality at the phosphorus atom. The mechanism proposed for this process involves the direct transfer of the N-*H* proton from one arm of the [NPNH] ligand to the other via the transition state that is illustrated in Scheme 2. Shifting of the phosphine ligand to the "bottom" of the metal and the close approach of the amine sidearm to the ruthenium center allows for the N-*H* proton to reside in a bridging position between both nitrogen atoms. Transfer of this proton from one arm to the other followed by dissociation of the resulting amine ligand and finally coordination of the phosphine back to the site *trans* to the olefin donor acts to invert the chirality of the phosphorus atom. A related transition state has been postulated for aryloxide/phenol proton exchange in a pentamethylcyclopentadienyl nickel(II) system.[48]

The solid-state molecular structure of complex *endo*-**3** shows that the amino hydrogen atom is pointed toward the amido nitrogen atom. Although the distance between the two nuclei (3.419 Å) is too long to be considered a hydrogen bond, the observed orientation

Scheme 2

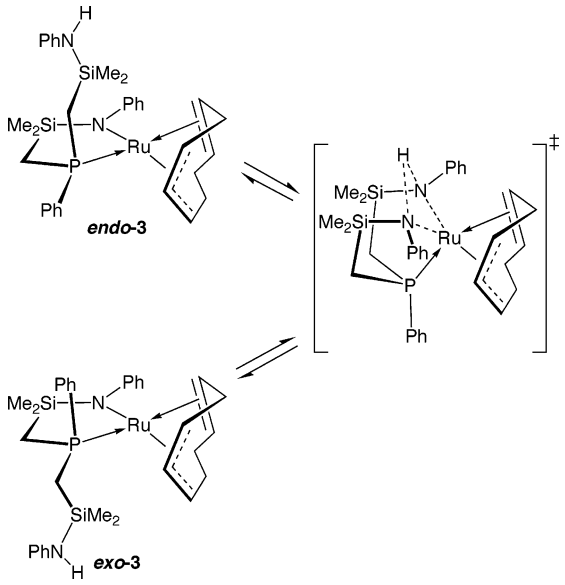

may be the result of an electrostatic attraction between these two nuclei. A hydrogen-bonding interaction was evident in the solid-state structure of the complex [P_2-NNH]Ru($C_6H_4PPh_2$) (**2**), with a NH···N distance of 2.404 Å.

The variable-temperature ^{1}H NMR data also permitted a kinetic investigation into the mechanistic details for the process that interconverts isomers *endo*-**3** and *exo*-**3**. Line-shape analysis of the N-*H* resonances allowed for the rate constants to be determined at several temperatures and used in an Eyring plot to calculate the activation parameters of $\Delta H^{\ddagger} = 16 \pm 1$ kcal mol^{-1} and $\Delta S^{\ddagger} = 4 \pm 4$ eu for this process (see Supporting Information).

Support for the proposed six-coordinate transition state shown in Scheme 2 comes from the structure of the stable and isolable lithium-ruthenate complexes. The addition of 1 equiv of LiN($SiMe_3$)$_2$ to an equilibrium mixture of *endo*-**3** and *exo*-**3** in toluene generates a hydrocarbon insoluble lithium-ruthenate complex, which upon addition of THF, results in the formation of [Li(THF)]([NPN]Ru(η^3: η^2-C_8H_{11})) (**4**), as shown in Scheme 3. The synthesis of the sodium-ruthenate complex is analogous to that of **4** but employs NaN($SiMe_3$)$_2$ as the base (see Supporting Information).

Figure 8 shows the solid-state molecular structure of complex **4** as determined by a single-crystal X-ray diffraction study. The solid-state structure of the sodium-ruthenate complex can be found in the Supporting Information. Selected bond lengths and angles for the lithium-ruthenate are given in Table 4.

Inspection of the solid-state molecular structure of complex **4** shows that the η^3-allyl, η^2-olefin coordination mode of the cyclooctadienyl ligand has been maintained and that the [NPN] ligand is bound to the ruthenium in a facial manner. The amido donors bridge the lithium and ruthenium centers, forming a "LiN_2Ru" core. Complex **4** is six-coordinate at ruthenium and exhibits C_1 symmetry in the solid state. Deviations from ideal octahedral coordination geometry arise due to constraints imposed by the chelating [NPN] ligand as well as the cyclooctadienyl ligand. For example, the P(1)–

(48) Holland, P. L.; Andersen, R. A.; Bergman, R. G.; Huang, J.; Nolan, S. P. *J. Am. Chem. Soc.* **1997**, *119*, 12800.

Scheme 3

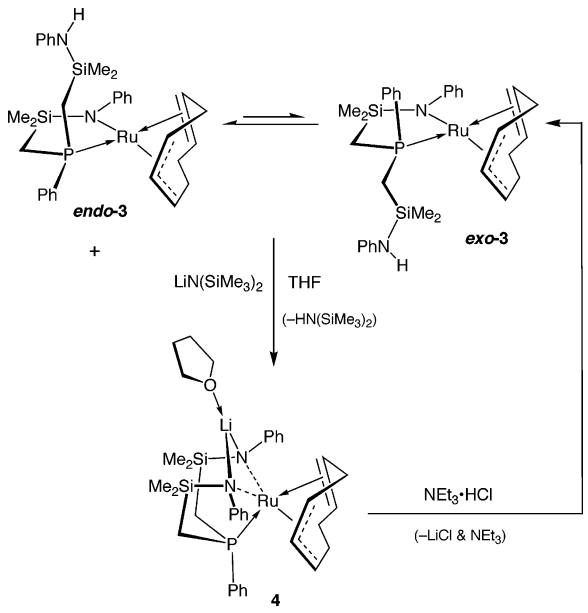

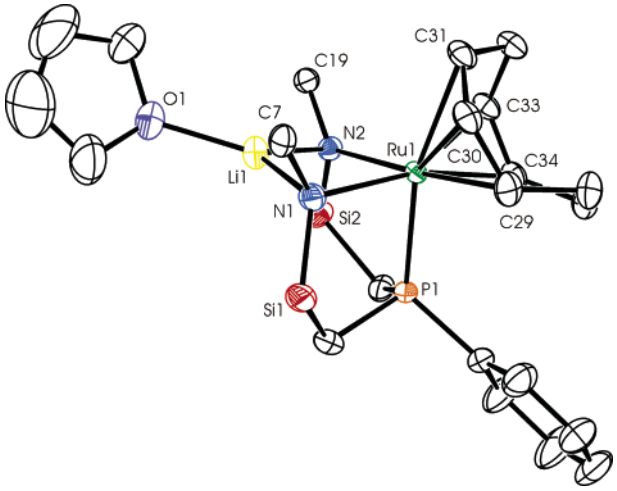

Figure 8. ORTEP representation (50% thermal ellipsoid probability) of the solid-state molecular structure of [Li(THF)]([NPN]Ru(η^3: η^2-C_8H_{11})) (**4**) as determined by X-ray diffraction. The [NPN] ligand silyl methyl groups have been omitted for clarity and only the *ipso* carbon atoms of the amido phenyl rings are shown.

Ru(1)−C(31) and N(2)−Ru(1)−C(31) bond angles (163.77(7)° and 110.04(8)°, respectively) show that the terminal allyl carbon atom, C(31), is bent away from its ideal apical position. In addition, atom C(31) is approximately 0.18 Å further displaced from the metal center than are C(29) and C(30) of the allyl donor. An unsymmetrical coordination mode for the cyclooctadienyl ligand in related ruthenium(II) systems has previously been reported.[37] The bis-amide-bridged "LiN_2Ru" core is asymmetric, containing one shorter (2.275(2) Å) and one longer (2.364(2) Å) ruthenium to nitrogen distance; the amido to lithium distances are equivalent within experimental error. The Ru−N bond lengths in **4** are longer than that found in *endo*-**3** (2.019(2) Å). Coordinative saturation at the ruthenium center does not allow for π-donation from the amido lone pair of electrons, and consequently both the amide donors exhibit a pseudo-tetrahedral coordination geometry.[49] The lithium atom in complex **4** adopts a planar, three-coordinate geometry with a molecule of THF completing its coordination sphere.

The asymmetry of **4** evident in the solid state is maintained in solution, which suggests a rigid solution structure. To support this, the $^{13}C\{^1H\}$ NMR spectrum contains four resonances for the silyl methyl carbon atoms and eight resonances for the inequivalent cyclooctadienyl carbon nuclei. Once again, the *J*-modulated $^{13}C\{^1H\}$ spectrum confirmed the η^3:η^2-coordination mode of the cyclooctadienyl ligand, as in complex **3**. The greatest variation in peak positions occurs for the ruthenium-bound carbon nuclei. The central allyl carbon (C_6), for instance, is shifted downfield from ca. δ 71.0 in *endo*-**3** and *exo*-**3** to δ 100.5 in complex **4**. The olefin carbon atom, C_2, experiences an upfield shift of similar magnitude from ca. δ 110.0 (in *endo*-**3** and *exo*-**3**) to δ 67.8.

Table 4. Selected Bond Lengths and Angles in the Complexes [Li(THF)]([NPN]Ru(η^3: η^2-C_8H_{11})) (4)

atom	atom	distance (Å)	atom	atom	distance (Å)
Ru(1)	N(1)	2.275(2)	N(2)	Li(1)	2.010(5)
Ru(1)	N(2)	2.364(2)	O(1)	Li(1)	1.956(5)
Ru(1)	P(1)	2.2944(6)	N(1)	C(7)	1.410(3)
Ru(1)	C(29)	2.179(2)	N(2)	C(19)	1.414(3)
Ru(1)	C(30)	2.176(2)	N(1)	Si(1)	1.745(2)
Ru(1)	C(31)	2.364(2)	N(2)	Si(2)	1.729(2)
Ru(1)	C(33)	2.180(2)	C(29)	C(30)	1.424(4)
Ru(1)	C(34)	2.224(2)	C(30)	C(31)	1.396(4)
N(1)	Li(1)	2.004(5)	C(33)	C(34)	1.384(4)

atom−atom−atom	angle (deg)	atom−atom−atom	angle (deg)
N(1)−Ru(1)−N(2)	86.49(7)	P(1)−Ru(1)−C(31)	163.77(7)
N(1)−Ru(1)−P(1)	87.12(5)	P(1)−Ru(1)−C(33)	113.17(7)
N(2)−Ru(1)−P(1)	84.28(5)	P(1)−Ru(1)−C(34)	81.44(8)
N(1)−Ru(1)−C(29)	97.13(9)	C(31)−Ru(1)−C(29)	66.6(1)
N(1)−Ru(1)−C(31)	100.97(8)	C(31)−Ru(1)−C(33)	62.87(9)
N(1)−Ru(1)−C(33)	156.22(8)	C(31)−Ru(1)−C(34)	88.8(1)
N(1)−Ru(1)−C(34)	167.14(9)	C(29)−Ru(1)−C(33)	92.1(1)
N(2)−Ru(1)−C(29)	175.46(9)	C(29)−Ru(1)−C(34)	78.9(1)
N(2)−Ru(1)−C(31)	110.04(8)	N(1)−Li(1)−N(2)	104.8(2)
N(2)−Ru(1)−C(33)	83.52(8)	Li(1)−N(1)−Ru(1)	84.5(2)
N(2)−Ru(1)-C(34)	98.12(9)	Li(1)−N(2)−Ru(1)	82.0(2)
P(1)−Ru(1)−C(29)	98.60(7)		

The ^{1}H NMR spectrum of **4** shows four silyl methyl resonances, four ligand methylene resonances, 11 inequivalent cyclooctadienyl proton resonances, and three sets of *ortho*, *meta*, and *para* phenyl proton resonances for the [NPN] phenyl groups. This number of peaks is consistent with a C_1 symmetric structure in solution. The changes in chemical shifts of the cyclooctadienyl protons (as compared to *endo*-**3** and *exo*-**3**) mirror those of the carbon nuclei to which they are attached (see Supporting Information).

As shown in Scheme 3, the equilibrium mixture of *endo*-**3** and *exo*-**3** can be regenerated by the stoichiometric addition of NEt_3·HCl to the ruthenate complex **4**. Utilizing the deuterium-labeled acid (NEt_3·DCl) in the above reaction allows for selective deuteration at the amine nitrogen atom, which verified the assignment of the N-*H* resonance in the ^{1}H NMR spectrum of the diastereomers *endo*-**3** and *exo*-**3**.

In analogy with the above example, in which the basic behavior of the lithium-ruthenate complex toward NEt_3·HCl regenerates the equilibrium mixture of *endo*-**3** and *exo*-**3**, the reaction of Me_3SiCl with **4** was examined. Addition of an excess of chlorotrimethylsilane (Me_3SiCl) to a solution of **4** in toluene results in a change in color from orange to red over a period of 24 h. After workup, the two diastereomers *endo*- and *exo*-[NPN(SiMe$_3$)]Ru(η^3:η^2-C_8H_{11}) (*endo*-**5** and *exo*-**5**, respectively) could be isolated as an extremely moisture-sensitive solid. The two isomers are formed in approximately 50% yield each; attempts to separate the two complexes via crystallization proved impossible.

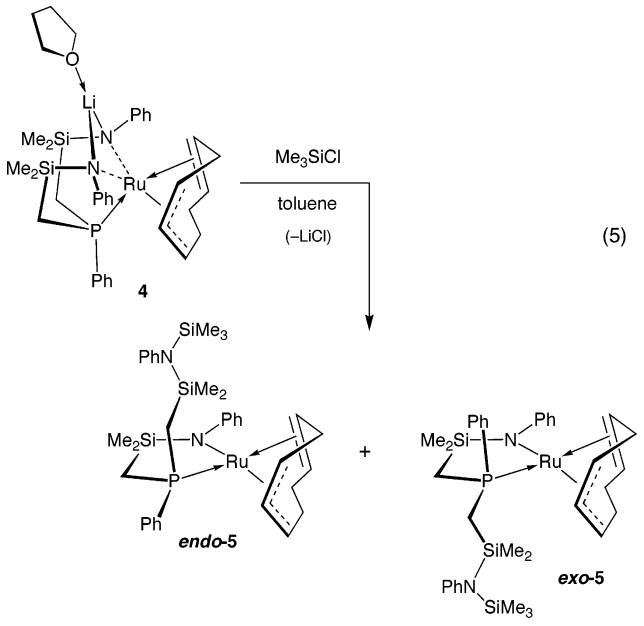

(5)

Unlike the room-temperature ^{1}H NMR spectrum for *endo*-**3** and *exo*-**3**, which is comprised of broadened peaks, the ^{1}H NMR spectrum (at 298 K) for complexes *endo*-**5** and *exo*-**5** contains well-resolved resonances for all proton environments, implying that the two species do not exhibit any fluxionality. In fact, examination of the ^{1}H and ^{31}P{^{1}H} NMR spectra as a function of temperature (from 200 to 360 K) shows that the two species are not in equilibrium since no change in product ratios could be discerned. These results provide further evidence for the mechanism depicted in Scheme 2 for the interconversion of the diastereomers of species **3**. As was expected, the bulky trimethylsilyl group is not exchanged between the two isomers, and consequently, they remain independent of one another.

The characterization of *endo*-**5** and *exo*-**5** was based on solution NMR studies. The ^{13}C{^{1}H} and ^{1}H NMR data were diagnostic for these two isomers and showed remarkable similarities to the corresponding low-temperature spectra of the diastereomeric mixture of *endo*-**3** and *exo*-**3**. The coupling of the ^{31}P nucleus to the olefinic carbon atoms indicates a *trans* disposition between the phosphine and olefin donors in these complexes. In *endo*-**5**, for example, C_1 occurs as a doublet at δ 61.6 ($^2J_{PC}$ = 6.3 Hz), and likewise C_2 appears as a doublet at δ 107.6 ($^2J_{PC}$ = 10.6 Hz). Complex *endo*-**3** shows very similar resonances for these two nuclei, with nearly identical coupling constants (6.5 and 10.5 Hz, respectively). A similar trend is observed for *exo*-**5** and *exo*-**3**. The ^{13}C chemical shifts of the remaining cyclooctadienyl carbon nuclei are only slightly shifted, suggesting that a very similar coordination mode is adopted by this ligand for the related *endo* and *exo* isomers of complexes **3** and **5**.

Both the *endo* and *exo* isomers of complex **5** have four ligand silyl methyl proton resonances; the ligand methylene resonances for both isomers overlap with the cyclooctadienyl resonances and occur between ca. δ 1.0 and 1.5. The terminal amino silyl methyl (N-Si*Me*$_3$) signal for *endo*-**5** occurs as a singlet at δ 0.15 and integrates for nine protons. For the isomer *exo*-**5** this resonance appears as a singlet at δ 0.12. The remaining phosphine, amine, and amido phenyl resonances occur at expected positions between δ 6.8 and 7.7. The ^{31}P{^{1}H} NMR spectrum contains two singlets at δ 32.9 and 32.3 for complexes *endo*-**5** and *exo*-**5**, respectively.

Summary and Conclusions

The synthesis of ruthenium(II) complexes that incorporate the mixed-donor macrocyclic [P_2N_2] and tridentate [NPN] ligand sets is described. The reaction of [P_2N_2]Li$_2$(Diox) with [RuCl$_2$(cod)]$_x$ generates the diamidodiphosphine complex [P_2N_2]Ru(η^2:η^2-C_8H_{12}) (**1**), which at room temperature displays C_{2v} symmetry in solution; however, cooling the solution results in a C_2 symmetric complex consistent with the solid-state X-ray structure. The reaction between the dilithium salt of the [P_2N_2] ligand with RuCl$_2$(PPh$_3$)$_3$ yields the species [P_2NNH]Ru($C_6H_4PPh_2$) (**2**), in which *ortho*-metalation of the triphenylphosphine ligand occurs. The solid-state molecular structure of **2** shows that there is an intramolecular hydrogen-bonding interaction involving the amine proton and amide nitrogen atom of the [P_2NNH] ligand. The position of amine proton in the coordination sphere suggests that this product results from thermodynamic rather than kinetic control.

The ligand [NPN]Li$_2$(THF)$_2$ reacts with [RuCl$_2$(cod)]$_x$ to give an equilibrium mixture of *endo*-**3** and *exo*-**3**. The diastereomers of **3** are formed via deprotonation of the cyclooctadiene moiety by the [NPN] ligand; transfer of the resulting amino proton between the [NPNH] side-

(49) (a) Conner, D.; Jayaprakash, K. N.; Gunnoe, T. B.; Boyle Paul, D. *Inorg. Chem.* **2002**, *41*, 3042. (b) Conner, D.; Jayaprakash, K. N.; Wells, M. B.; Manzer, S.; Gunnoe, T. B.; Boyle, P. D. *Inorg. Chem.* **2003**, *42*, 4759.

arms establishes the observed equilibrium. Deprotonation of co-ligands would appear to be a common occurrence in ruthenium(II) systems containing the [NPN] and $[P_2N_2]$ ligand sets. Formation of the ruthenate complex [Li(THF)]([NPN]Ru(η^3:η^2-C_8H_{11})) (**4**) is accomplished by the addition of $LiN(SiMe_3)_2$ to a mixture of *endo*-**3** and *exo*-**3**. The ruthenate species is nonfluxional in solution, as evidenced by the NMR data. Complex **4** reacts with acidic compounds to regenerate an equilibrium mixture of *endo*-**3** and *exo*-**3** or with chlorotrimethylsilane to give the two independent, nonfluxional diastereomers *endo*- and *exo*-[NPN($SiMe_3$)]-Ru(η^3:η^2-C_8H_{11}) (*endo*-**5** and *exo*-**5**, respectively).

Experimental Section

General Procedures. Unless otherwise stated, all manipulations were performed under a dry, oxygen-free atmosphere of dinitrogen or argon by means of standard Schlenk or glovebox techniques (Vacuum Atmospheres HE-553-2 glovebox equipped with a MO-40-2H purification system and a −40 °C freezer). Toluene and hexanes were purchased in anhydrous form from Aldrich and deoxygenated by passage through a tower containing Q-5 catalyst and further dried by passage through a tower containing alumina under a positive pressure of dinitrogen. Anhydrous THF was predried by refluxing over CaH_2 and then distilled under argon from sodium benzophenone ketyl. Anhydrous diethyl ether was stored over sieves and distilled from sodium benzophenone ketyl under argon. Deuterated benzene, tetrahydrofuran, pentane, and toluene were dried by refluxing over sodium and potassium alloy in a sealed vessel under partial pressure, then trap-to-trap distilled and degassed by three freeze−pump−thaw cycles prior to use. Nitrogen and argon were dried and deoxygenated by passage through a column containing activated molecular sieves and MnO. Unless otherwise stated, ^{1}H, ^{1}H{^{31}P}, ^{2}H, ^{31}P{^{1}H}, ^{13}C{^{1}H}, ^{7}Li{^{1}H}, and variable-temperature NMR spectra were recorded on a Bruker AMX-500 instrument operating at 500.1 MHz for ^{1}H spectra, a Bruker AV-300 instrument (300.1 MHz), or a Bruker AC-200 instrument (200.1 MHz). ^{1}H NMR spectra were referenced to internal C_6D_5H (7.15 ppm) or C_7D_7H (2.09 ppm), ^{31}P{^{1}H} NMR spectra to external $P(OMe)_3$ (141.0 ppm with respect to 85% H_3PO_4 at 0.0 ppm), and ^{13}C{^{1}H} NMR spectra to $^{13}CC_5D_6$ (128.4 ppm). All δ values are given in ppm units. Infrared spectra were recorded on an ATI Matton Genesis Series FTIR spectrometer as KBr pellets. Elemental analyses were performed in the Department of Chemistry at the University of British Columbia by Mr. P. Borda or Mr. M. Lakha. Complexes for which elemental data are not reported gave results outside of error limits. For this reason, these derivatives were characterized by solution and X-ray data only.

(i) Materials. The compounds $[NPN]Li_2(THF)_2$,[22] $[P_2N_2]Li_2$(Diox),[23] $[RuCl_2(cod)]_x$,[50] and $RuCl_2(PPh_3)_3$[51] were prepared according to reported literature procedures. NEt_3·DCl was prepared by the dropwise addition of aqueous deuterium chloride to a solution of triethylamine in diethyl ether. The solid was collected by filtration and dried under vacuum. Triphenylphosphine, triisopropylphosphine, and tricyclohexylphosphine (Strem Chemicals) and $LiN(SiMe_3)_2$, $NaN(SiMe_3)_2$, NEt_3·HCl, CuCl, and chlorotrimethylsilane (Aldrich) were used without further purification. $RuCl_3$·$3H_2O$ was obtained on loan from Johnson-Matthey, as well as purchased from Precious Metals Online.

$[P_2N_2]$Ru(η^2:η^2-C_8H_{12}) (1). A solution of $[P_2N_2]Li_2$(Diox) (0.734 g, 1.16 mmol) in 10 mL of THF was added to a slurry of $[RuCl_2(cod)]_x$ (0.324 g, 1.16 mmol) in 10 mL of THF. The mixture was stirred at room temperature for 3 h, yielding a yellow-brown solution. The mixture was evaporated to dryness in vacuo, and the resulting solid was extracted into 20 mL of toluene and filtered through Celite. The solvent was removed until a thick oily residue remained. Addition of hexanes (10 mL) caused a yellow solid to precipitate from the solution. The solid was collected on a frit and washed with hexanes until the dark impurities were removed. The remaining solid was dried under vacuum to yield $[P_2N_2]$Ru(η^2:η^2-C_8H_{12}) (**1**) (0.628 g, ∼70%). X-ray quality crystals were obtained by the slow evaporation of the hexanes rinsings and contained 1 equiv of cocrystallized hexane. ^{1}H NMR (C_6D_6, 298 K, 500 MHz): δ 0.40 and 0.50 (s, SiCH_3, 24H total), 0.95 and 1.42 (m (br), P-CH_2, 8H total), 1.82 (m, cyclooctadiene −CH_2, 8H), 2.80 (s (br), cyclooctadiene −C*H*, 4H), 7.12 (m, overlapping, PPh-*para*, 1H), 7.20 (m, PPh-*meta*, 4H), (m, PPh-*ortho*, 4H). ^{31}P{^{1}H} NMR (C_6D_6, 298 K, 202.5 MHz): δ 44.5 (s). ^{13}C{^{1}H} NMR (C_6D_6, 298 K, 125.8 MHz): δ 7.0 and 9.0 (s, SiCH_3), 25.0 (s (br), cyclooctadiene −CH_2), 28.0 (s (br), P-CH_2), 70.0 (s, cyclooctadiene −C*H*), 127.5 (s, overlapping, PPh-*para*), 128.5 (s, PPh-*meta*), 131.0 (s, PPh-*ortho*), 143.0 (s (br), PPh-*ipso*). ^{1}H NMR (C_6D_6, 198 K, 500 MHz): δ 0.30 to 0.60 (s, overlapping, SiCH_3, 24H total), 0.90 (s (br), P-CH_2, 2H), 1.30 (s (br), overlapping, P-CH_2 2H), 1.30 (s (br), overlapping, cyclooctadiene −CH_2, 2H), 1.90 (s, cyclooctadiene −CH_2, 2H), 2.09 (s, cyclooctadiene −CH_2, 2H), 2.20 (s, cyclooctadiene −CH_2, 2H), 2.60 (s (br), cyclooctadiene −C*H*, 2H), 3.00 (s (br), cyclooctadiene −C*H*, 2H), 6.80 to 7.15 (m, overlapping, PPh-*meta* and *-para*, 6H total), 7.80 (s (br), PPh-*ortho*, 4H).

^{1}H NMR (C_7D_8, 212 K, 500 MHz): δ 2.60 and 3.0 (s (br), cyclooctadiene −C*H*, 2H). Line shape analysis of the peaks at different temperatures gave rate constants that when plotted using the Arrhenius equation have $E_a = 18.6 \pm 1.6$ kcal/mol (see Supporting Information).

Despite many attempts, a satisfactory elemental analysis could not be obtained for this material.

$[P_2NNH]$Ru($C_6H_4PPh_2$) (2). Toluene (30 mL) was added to a mixture of $[P_2N_2]Li_2$(Diox) (0.170 g, 0.268 mmol) and $RuCl_2(PPh_3)_3$ (0.256 g, 0.267 mmol). The initial slurry was stirred for 3 h at room temperature, resulting in the formation of an orange-brown solution, which was filtered to remove insoluble LiCl. Anhydrous CuCl (0.054 g, 0.536 mmol) was added to the solution, and the contents were stirred for 12 h. The mixture was filtered, and the filtrate was evaporated until approximately 2 mL of toluene remained. Addition of pentane (10 mL) caused the deposition of $[P_2NNH]$Ru($PC_6H_4Ph_2$) (**2**) as an orange solid. The solid was collected by filtration, rinsed with a minimum amount of pentane, and dried in vacuo to yield 0.207 g of **2** (86%). Single crystals suitable for an X-ray diffraction study were grown by the slow evaporation of the pentane-soluble rinsings. There were two independent molecules in the asymmetric unit as well as a molecule of cocrystallized pentane. ^{1}H NMR (C_6D_6, 298 K, 500 MHz): δ 0.39, 0.41, 0.58, and 0.60 (s, SiCH_3, 24H total), 1.40 (m, overlapping, P-CH_2, 4H), 1.53 (m, overlapping, P-CH_2, 4H), 2.80 (s, N-*H*), 6.52−8.12 (m, P-*Ph*, $[P_2NNH]$ and $PC_6H_4Ph_2$, 24 H total). ^{31}P{^{1}H} NMR (C_6D_6, 298 K, 202.5 MHz): δ 25.8 (d, $^2J_{PP} = 31$ Hz, $[P_2NNH]$, 2P), −11.8 (t, $^2J_{PP} = 31$ Hz, $PC_6H_5Ph_2$, 1P). Anal. Calcd for $C_{42}H_{57}N_2P_3Si_4Ru$: C, 56.28; H, 6.41; N 3.13. Found: C, 56.11; H, 6.58; N, 3.29.

*For complexes **3** through **5** the following labeling convention is employed for assignment of the ^{1}H and ^{13}C nuclei of the cyclooctadienyl moiety:*

***endo*- and *exo*-[NPNH]Ru(η^3:η^2-C_8H_{11}) (*endo*-3 and *exo*-3).** Toluene (30 mL) was added to a mixture of $[NPN]Li_2(THF)_2$ (1.06 g, 1.78 mmol) and $[RuCl_2(cod)]_x$ (0.50 g, 1.78 mmol), and the mixture was stirred for 2 days at room temperature. During this time the initial brown slurry turned red and a colorless solid formed. The mixture was then filtered through Celite and the solvent removed under reduced pressure,

(50) Albers, M. O.; Ashworth, T. V.; Oosthuizen, E. *Inorg. Synth.* **1989**, *26*, 68.
(51) Hallman, P. S.; Stephenson, T. A.; Wilkinson, G. *Inorg. Synth.* **1970**, *12*, 237.

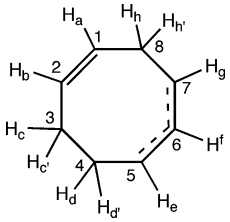

leaving an oily solid. A small amount of hexanes (ca. 5 mL) was added to dissolve the solid, and the mixture was allowed to stand in a closed vessel for 48 h, during which time complex **3** crystallizes from solution. The supernatant was decanted and the red crystals were washed with hexanes. Yield: 0.90 g, 78%. A further crop of crystals was obtained by the slow evaporation of the supernatant. Isomer *endo*-**3**: ^{1}H NMR (C_7D_8, 245 K, 500 MHz): δ 0.08 (s, br, SiCH_3, 6H), 0.34 (s, SiCH_3, 3H), 0.43 (s, SiCH_3, 3H), δ 0.76 (m, AA′BX, PCHH, 1H), 1.0 (m, AA′BX, PCH_2, 2H), 1.17 (m, AA′BX, PCHH, 1H), 1.50 (m, CH$_d$H$_d$′, 1H), 1.58 (m, CH$_c$H$_c$′, 1H), 1.64 (m, C$H$$_f$, 1H), 2.00 (m, CH$H_h$′, 1H), 2.18 (m, C$H_dH_d$′, 1H), 2.36 (m, C$H_cH_c$′, 1H), 2.70 (m, C$H_hH_h$′, 1H), 2.85 (m, C$H_g$, 1H), 4.20 (m, C$H_e$, 1H), 4.23 (m, C$H_a$, 1H), 4.25 (m, C$H_b$, 1H), 6.63 (s, N$H$, 1H), 6.82−7.42 (m, overlapping, NPh, NHPh, and PPh,). ^{31}P{^{1}H} NMR (C_7D_8, 245 K, 202.5 MHz): δ 33.4 (s). ^{13}C{^{1}H} NMR (C_7D_8, 245 K, 125.8 MHz) selected peaks: δ 25.2 (s, C_8), 30.3 (s, C_3), 32.8 (s, C_4), 35.6 (s, C_7), 61.4 (d, C_1, $^2J_{PC}$ = 6.5 Hz), 61.6 (s, C_5), 71.6 (s, C_6), 108.1 (d, C_2, $^2J_{PC}$ = 10.5 Hz). Isomer *exo*-**3**: ^{1}H NMR (C_7D_8, 245 K, 500 MHz): δ 0.09 (s, overlapping, SiCH_3, 3H), 0.28 (s, SiCH_3, 3H), 0.32 (s, overlapping, SiCH_3, 6H), 0.85 (m, overlapping, AA′BX, PCH_2, 2H), 1.0 (m, overlapping, AA′BX, PCH_2, 2H), 1.30 (m, CH$_c$H$_c$′, 1H), 1.50 (m, overlapping, C$H$$_f$, 1H), 1.75 (m, CH$_dH_d$′, 1H), 1.83 (m, C$H_cH_c$′, 1H), 2.15 (m, overlapping, CH$_h$H$_h$′, 1H), 2.20 (m, CH_dH$_d$′, 1H), 3.09 (m, CH_hH$_h$′, 1H), 3.37 (m, CH_g, 1H), 3.50 (m, CH_e, 1H), 3.92 (m, CH_b, 1H), 4.68 (m, CH_a, 1H), 6.35 (s, NH, 1H), 6.82−7.42 (m, overlapping, NPh, NHPh, and PPh). $^3J_{ab}$ = 7.80 Hz, $^3J_{ah}$ = 7.70 Hz, $^3J_{ah}$′ = 7.30 Hz, $^3J_{bc}$ = 6.20 Hz, $^3J_{bc}$′ = 6.10 Hz, $^2J_{cc}$′ = 14.60 Hz, $^3J_{cd}$ = 7.60 Hz, $^3J_{cd}$′ = 6.00 Hz, ^3J_c′$_d$ = 7.20 Hz, ^3J_c′$_d$′ = 8.60 Hz, $^2J_{dd}$′ = 17.0 Hz, $^3J_{de}$ = 5.60 Hz, ^3J_d′$_e$ = 5.80 Hz, $^3J_{ef}$ = 8.00 Hz, $^3J_{fg}$ = 9.90 Hz, $^3J_{gh}$ = 7.90 Hz, $^3J_{gh}$′ = 4.20 Hz, $^2J_{hh}$′ = 19.30 Hz. ^{31}P{^{1}H} NMR (C_7D_8, 245 K, 202.5 MHz): δ 32.9 (s). ^{13}C{^{1}H} NMR (C_7D_8, 245 K, 125.8 MHz) selected peaks: δ 26.6 (s, C_8,), 27.0 (s, C_3), 36.3 (s, C_4), 36.5 (s, C_7), 64.9 (s, C_5), 65.3 (d, C_1, $^2J_{PC}$ = 5.8 Hz), 70.8 (s, C_6), 110.0 (d, C_2, $^2J_{PC}$ = 11.3 Hz). IR (KBr): ν(NH) at 2945 and 2906 cm^{-1}. Anal. Calcd for $C_{32}H_{43}N_2PRuSi_2$: C, 59.69; H, 6.73; N, 4.35. Found: C, 59.68; H, 7.09; N, 4.35.

[Li(THF)]([NPN]Ru(η^3:η^2-C_8H_{11})) (4). A solution of LiN(SiMe$_3$)$_2$ (0.064 g, 0.384 mmol) in toluene (10 mL) was added dropwise to a toluene solution of **3** (0.247 g, 0.384 mmol) (20 mL), and the mixture was stirred at room temperature for 3 h, during which time an orange solid precipitated from the solution. The solvent was removed under reduced pressure until half volume, and hexanes (20 mL) was added to ensure complete precipitation. The orange solid is insoluble in aromatic solvents. THF was added to a mixture of the orange solid in toluene until it completely dissolved. Removal of the volatiles in vacuo and addition of hexanes caused the deposition of **3** as an orange microcrystalline solid. The solid was filtered, washed with hexanes, and dried under vacuum. Yield: 0.255 g, 92%. X-ray quality crystals were grown by the slow evaporation of a saturated toluene solution. ^{1}H NMR (C_6D_6, 298 K, 500 MHz): δ 0.10, 0.20, 0.35, and 0.50 (s, SiCH_3, 12 total), 1.00 (m, AA′BX, PCHH, 1H), 1.07 (m, CH$_c$H$_c$′, 1H), 1.14 (m, overlapping, OCH$_2$CH_2, 2H), 1.18 (m, overlapping, CH_cH$_c$′, 1H), 1.33 (m, CH$_d$H$_d$′, 1H), 1.44 (m, AA′BX, PCHH, 1H), 1.65 (m, AA′BX, PCHH, 1H), 1.73 (m, overlapping, AA′BX, PCHH, 1H), 1.76 (m, CH_dH$_d$′, 1H), 2.17 (m, CH_a, 1H), 2.29 (m, CH_b, 1H), 2.50 (m, CHH_h′, 1H), 3.06 (m, overlapping, OCH_2-CH$_2$, 2H), 3.10 (m, overlapping, CH_e, 1H), 3.45 (m, overlapping, CH_hH$_h$′, 1H), 3.45 (m, overlapping, C$H$$_f$, 1H), 4.35 (m, C$H_g$, 1H), 6.58 (t, NPh-*para*, 1H), 6.78 (t, N′Ph-*para*, 1H), 7.70 (m, NPh-*meta*, 2H), 7.20 (m, overlapping, NPh-*ortho*, 2H), 7.20 (m, overlapping, PPh-*para*, 1H), 7.39 (m, N′Ph-*meta*, 2H), 8.05 (m, AX, PPh-*ortho*, 2H), 8.30 (d, N′Ph-*ortho*, 2H). ^{31}P{^{1}H} NMR (C_6D_6, 298 K, 202.5 MHz): δ 46.8 (s). ^{13}C{^{1}H} NMR (C_7D_8, 298 K, 125.8 MHz) selected data: δ 22.7 (s, C_8), 27.7 (s, C_4), 27.9 (s, C_3), 33.2 (d, C_1, $^2J_{PC}$ = 6.4 Hz), 45.0 (d, C_7, $^2J_{PC}$ = 19.2 Hz), 46.0 (d, C_5, $^2J_{PC}$ = 2.1 Hz), 68.2 (d, C_2, $^2J_{PC}$ = 5.8 Hz), 100.5 (s, C_6).

The sodium congener is described in the Supporting Information.

Reaction of Complex 4 with NEt$_3$·HCl. Addition of NEt$_3$·HCl (0.015 g, 0.109 mmol) to a solution of **4** (0.078 g, 0.108 mol) in toluene (10 mL) resulted in a change in color from orange to red within 2 h. The mixture was filtered to remove insoluble LiCl, and the volatile components were removed under vacuum, giving a red solid. The ^{1}H and ^{31}P{^{1}H} NMR spectra of the red solid indicate that it is a mixture of the two diastereomers *endo*-**3** and *exo*-**3**.

Reaction of Complex 4 with NEt$_3$·DCl. A procedure similar to that described above for the reaction with NEt$_3$·HCl was followed: NEt$_3$·DCl (0.017 g, 0.123 mmol), **4** (0.086 g, 0.119 mmol), and toluene (10 mL). The ^{1}H and ^{31}P{^{1}H} NMR spectra indicate the formation of an equilibrium mixture of *endo*-**3**-d_1 and *exo*-**3**-d_1 in which deuteration at the amino site occurs.

***endo*- and *exo*-[NPN(SiMe$_3$)]Ru(η^3:η^2-C_8H_{11}) (*endo*-5 and *exo*-5).** A 10-fold excess of chlorotrimethylsilane (0.292 g, 2.69 mmol) was added to an orange solution of **4** (0.194 g, 0.269 mmol) in toluene (30 mL). Over the period of 48 h the solution turns red with the formation of a white solid (LiCl). The solvent and other volatiles were removed in vacuo. Toluene was added to the remaining solid, and the mixture was filtered to remove insoluble byproducts. The soluble fraction was dried under vacuum to give a mixture of *endo*-**5** and *exo*-**5** as a red solid material (0.17 g, 88%). Attempts to separate the two isomers by fractional crystallization proved unsuccessful. This material was characterized spectroscopically. Isomer *endo*-**5**: ^{1}H NMR (C_6D_6, 298 K, 500 MHz): δ 0.12 (s, overlapping, SiCH_3, 3H), 0.15 (s, overlapping, terminal N-SiCH_3), 0.18 (s, overlapping, SiCH_3), 0.33 (s, SiCH_3, 3H), 0.46 (s, SiCH_3, 3H), 1.00 to 1.50 (m, overlapping, P-CH_2), 1.47 (m, CH$_c$H$_c$′, 1H), 1.52 (m, C$H$$_f$, 1H), 1.85 (m, CH$_dH_d$′, 1H), 2.05 (m, CH$H_h$′, 1H), 2.10 (m, C$H_cH_c$′, 1H), 2.25 (m, C$H_dH_d$′, 1H), 2.77 (m, C$H_hH_h$′, 1H), 2.90 (m, C$H_g$, 1H), 4.00 (m, C$H_b$, 1H), 4.16 (m, C$H_e$, 1H), 4.25 (m, C$H_a$, 1H), 6.80−7.45 (m, overlapping, NPh, NHPh, and PPh). ^{31}P{^{1}H} NMR (C_7D_8, 298 K, 202.5 MHz): δ 32.9 (s). ^{13}C{^{1}H} NMR (C_7D_8, 298 K, 125.8 MHz) selected peaks: δ 25.5 (s, C_8), 28.5 (s, C_3), 35.0 (s, C_4), 35.6 (s, C_7), 61.6 (d, C_1, $^2J_{PC}$ = 6.3 Hz), 61.8 (s, C_5), 70.1 (s, C_6), 107.6 (d, C_2, $^2J_{PC}$ = 10.6 Hz). Isomer *exo*-**5**: ^{1}H NMR (C_7D_8, 298 K, 500 MHz): δ 0.12 (s, overlapping, terminal N-SiCH_3), 0.13 (s, overlapping, SiCH_3, 3H), 0.16 (s, overlapping, SiCH_3), 0.57 (s, SiCH_3, 3H), 0.60 (s, SiCH_3, 3H), 1.00 to 1.50 (m, overlapping, P-CH_2), 1.43 (m, overlapping, C$H$$_f$, 1H), 1.45 (m, CH$_cH_c$′, 1H), 1.75 (m, CH$_dH_d$′, 1H), 2.08 (m, C$H_cH_c$′, 1H), 2.12 (m, C$H_dH_d$′, 1H), 2.20 (m, overlapping, CH$_h$H$_h$′, 1H), 2.95 (m, CH_hH$_h$′, 1H), 3.27 (m, CH_g, 1H), 3.60 (m, CH_e, 1H), 3.87 (m, CH_b, 1H), 4.50 (m, CH_a, 1H), 6.80−7.45 (m, overlapping, NPh, NHPh, and PPh). ^{31}P{^{1}H} NMR (C_7D_8, 298 K, 202.5 MHz): δ 32.3 (s). ^{13}C-{^{1}H} NMR (C_7D_8, 298 K, 125.8 MHz) selected peaks: δ 26.5 (s, C_8), 26.9 (s, C_3), 36.2 (s, C_7), 36.9 (s, C_4), 62.9 (d, C_1, $^2J_{PC}$ = 5.9 Hz), 63.7 (s, C_5), 69.9 (s, C_6), 108.1 (d, C_2, $^2J_{PC}$ = 11.6 Hz).

Acknowledgment. Funding for this research was provided by NSERC of Canada (Discovery Grant to M.D.F.).

Supporting Information Available: Crystallographic data in CIF format for all complexes. Additional NMR data for complexes (VT and simulation data); calculated rate constants, equilibrium constants for selected complexes; full experimental details for the synthesis of [Na(THF)]-([NPN]Ru(η^3:η^2-C_8H_{11})) including X-ray data and the ORTEP diagram; experimental details for X-ray data collection and refinement for all of the complexes. This material is available free of charge via the Internet at http://pubs.acs.org.

OM050574I